

Landscape controls on the timing of spring, autumn, and growing season length in mid-Atlantic forests

ANDREW J. ELMORE*, STEVEN M. GUINN*, BURKE J. MINSLEY† and ANDREW D. RICHARDSON‡

*Appalachian Laboratory, University of Maryland Center for Environmental Science, 301 Braddock Rd, Frostburg, MD USA,

†United States Geological Survey, Crustal Geophysics and Geochemistry Science Center, Denver, CO USA, ‡Department of Organismic & Evolutionary Biology, Harvard University, Cambridge, MA USA

Abstract

The timing of spring leaf development, trajectories of summer leaf area, and the timing of autumn senescence have profound impacts to the water, carbon, and energy balance of ecosystems, and are likely influenced by global climate change. Limited field-based and remote-sensing observations have suggested complex spatial patterns related to geographic features that influence climate. However, much of this variability occurs at spatial scales that inhibit a detailed understanding of even the dominant drivers. Recognizing these limitations, we used nonlinear inverse modeling of medium-resolution remote sensing data, organized by day of year, to explore the influence of climate-related landscape factors on the timing of spring and autumn leaf-area trajectories in mid-Atlantic, USA forests. We also examined the extent to which declining summer greenness (greendown) degrades the precision and accuracy of observations of autumn offset of greenness. Of the dominant drivers of landscape phenology, elevation was the strongest, explaining up to 70% of the spatial variation in the onset of greenness. Urban land cover was second in importance, influencing spring onset and autumn offset to a distance of 32 km from large cities. Distance to tidal water also influenced phenological timing, but only within ~5 km of shorelines. Additionally, we observed that (i) growing season length unexpectedly increases with increasing elevation at elevations below 275 m; (ii) along gradients in urban land cover, timing of autumn offset has a stronger effect on growing season length than does timing of spring onset; and (iii) summer greendown introduces bias and uncertainty into observations of the autumn offset of greenness. These results demonstrate the power of medium grain analyses of landscape-scale phenology for understanding environmental controls on growing season length, and predicting how these might be affected by climate change.

Keywords: forest phenology, growing season length, inverse modeling, remote sensing

Received 31 May 2011; revised version received 21 July 2011 and accepted 4 August 2011

Introduction

One of the largest, most easily predicted, and already documented biological impacts of climate change on temperate ecosystems is a lengthening of the growing season (Menzel & Fabian, 1999; Field *et al.*, 2007). In summer-active/winter-dormant systems, the timing of spring and autumn has a profound impact on the water, carbon, and energy balance of forests, grasslands, and agricultural fields (Parmesan & Yohe, 2003; Liang & Schwartz, 2009; Morisette *et al.*, 2009). In particular, a longer growing season, which has already been detected in remote sensing time series for some regions (Myneni *et al.*, 1997; Zhang *et al.*, 2007), might be expected to increase carbon uptake by temperate forests, providing an important negative feedback to

greenhouse gas concentrations and global warming (Baldocchi & Wilson, 2001; Chapin *et al.*, 2008). However, if belowground resources become more limiting or if warmer temperatures stimulate heterotrophic respiration, the impact of a longer growing season will be reduced (Gu *et al.*, 2003; White & Nemani, 2003; Morisette *et al.*, 2009; Noormets, 2009; Richardson *et al.*, 2009b, 2010; Zhao & Running, 2010). Understanding landscape and climatic controls on the trajectory of leaf area development, summer maturity, and senescence is therefore key to understanding the impact of feedback processes and ecosystem response to climate change.

The nature of phenological patterns in spring and autumn is dependent on the scale of observation, which strongly determines the suite of environmental parameters influencing phenological timing. At continental scales, growing season length is predicted well by climatic gradients associated with latitude, longitude, and elevation (Hopkins, 1918; Fitzjarrald *et al.*, 2001). Common garden experiments have also demonstrated

Correspondence: Andrew J. Elmore, Appalachian Laboratory, 301 Braddock Rd., Frostburg, MD 21532, USA, tel. +1 (301) 689 7124, fax +1 (301) 689 7200, e-mail: aelmore@umces.edu

a direct effect of photoperiod (as expressed by latitudinal differences) on spring phenological timing for some species (Lechowicz, 1984). At smaller scales, spatial patterns are likely more complex, incorporating a greater range of processes. For example, urban heat islands (Imhoff *et al.*, 2010) have been shown to lead to an earlier start of spring in some areas of the world (Zhang *et al.*, 2004; Fisher *et al.*, 2006), but not all (Gazal *et al.*, 2008). Climate moderation due to large water bodies has been related to a later spring onset of greenness, and even microclimatic patterns related to cold air drainage into small valleys have been shown to influence the timing of the spring onset (Fisher *et al.*, 2006). Fine scale variability in phenological timing can be due to species effects (Liang *et al.*, 2011), with the phenology of individual tree species consistently either preceding or lagging other species despite up to 3 weeks inter-annual variation (Richardson & O'Keefe, 2009).

Remote sensing data are widely considered to provide a source for consistent phenological measurements across space and time. However, observed trends in growing season length are highly sensitive to the observation and algorithm used to identify the start and end of the growing season (White *et al.*, 2009). Of the many studies investigating changes in phenology (e.g. Myrneni *et al.*, 1997; Schwartz *et al.*, 2006), the vast majority have focused on the start of spring or have used the same methodology to identify both ends of the growing season (Robeson, 2002; Christidis *et al.*, 2007; Vitasse *et al.*, 2009). In general, studies that have examined both spring and autumn timing have concluded that both are important to global change research due to differing effects on ecosystem metabolism (Ahas *et al.*, 2002; Chmielewski & Rotzer, 2002; Piao *et al.*, 2007; Piao *et al.*, 2008). However, a gradual summer 'green down' seen in most remote sensing timeseries of forest canopy greenness (Jenkins *et al.*, 2007; Friedl *et al.*, 2010) presents a challenge to resolving the timing of autumn from remote sensing timeseries. Vegetation indices characterizing reflectance in the visible green or the strength of near-infrared reflectance relative to visible (e.g. the Normalized Difference Vegetation Index, NDVI) typically rise to a peak in late spring, at which point a two-stage decline begins: several months of gradually decreasing greenness, beginning as early as late June, are followed by a more rapid drop-off in autumn, related to leaf senescence and abscission. Because the autumn greenness trajectory is more gradual than it is in spring, estimates of the end of season are inherently more uncertain (Ganguly *et al.*, 2010).

Beyond accounting for summer greendown, a second limitation to understanding mechanisms determining phenological timing using remote sensing concerns the need for higher spatial resolution measurements.

Coarse resolution sensors such as the Moderate Resolution Imaging Spectrometer (MODIS) are inadequate for detecting fine-scale variability in the onset or offset of greenness due to microclimatological patterns that are obscured by the large pixel sizes. Recently, methods have been developed to calculate average phenology at medium spatial resolution (Fisher *et al.*, 2006). These methods involve analyzing stacks of many medium-resolution satellite images, organized by day of year (DOY) and discarding the year of acquisition. Measurements of vegetation from each image are then used to fit an average phenology curve. The resulting average date of the onset of greenness has been validated against field data (Fisher *et al.*, 2006), spatially aggregated and compared against measurements from lower-resolution data (Fisher & Mustard, 2007), and compared with predictions from phenology models (Fisher *et al.*, 2007). Such observations provide valuable information regarding spatial patterns in the average land surface phenology, but do not directly lend themselves to monitoring the effects of climate change over time.

The objectives of this paper were to (i) develop and quantify the uncertainty of a phenology curve-fitting algorithm that accounts for declining greenness throughout the summer growing season, here termed 'greendown'; (ii) apply this algorithm at a spatial grain appropriate for the study of individual forest stands; and (iii) use the derived estimates of spring onset and autumn offset of greenness and growing season length to explore landscape patterns in phenological timing. Due to mixed pixel effects, we saw the need for observations of growing season length made at a significantly smaller spatial grain than what is routinely used in remote sensing phenology research. We apply the method to a highly fragmented landscape, in the mid-Atlantic region of the United States, which is undergoing considerable pressure from land-use (Lookingbill *et al.*, 2009; Elmore & Guinn, 2010) and climate changes (Najjar *et al.*, 2010).

Methods

Site description

The study region chosen for this work is defined by the boundary of the Landsat path 15/row 33, which spans a latitude range from 39.87 to 37.95°N and longitude from -77.75 to -76.16°W. The Chesapeake Bay and its tidal tributaries dominate the eastern portion of the study region. The study region spans three different physiographic regions: the Coastal Plain, the Piedmont Plateau, and the Blue Ridge Mountains. Each physiographic region has distinct landscape characteristics that justify studying each in isolation. The Coastal Plain is a relatively flat region extending from tidal shorelines to the geographically important 'fall line', which

designates the border with the Piedmont Plateau, where streams abruptly drop from the Piedmont Plateau to the Coastal Plain. The Piedmont Plateau exhibits significantly greater topographic variation than the Coastal Plain. Early development in the mid-Atlantic focused on the fall line due to the accessibility of hydraulic power in these areas. Where the fall line met tidal waters appropriate for developing deep-water ports, dense urban societies emerged. Today, the cities of Baltimore and Washington DC are the dominate urban centers in the region with a combined metropolitan regional population of 8.2 million. Forests of the coastal plain and piedmont plateau are fragmented by agriculture and suburban expansion, leaving approximately 40% of forest intact. The Blue Ridge lies to the west of the Piedmont and remains largely forested. Elevation along the Blue Ridge summit is ~500 m above the surrounding piedmont, constituting the largest elevation gradient in the study region.

The native land cover of the mid-Atlantic region (spanning the eastern states from New York to Virginia) is primarily deciduous forest, roughly 80% of which falls into two forest categories, Oak-Hickory and Maple-beech-birch (Jenkins *et al.*, 2001). Forests in the state of Maryland, upon which our study region is centered, are composed of 90% deciduous hardwood species (Brown *et al.*, 1999), such as hickory (*Carya* spp.), Tulip poplar (*Liriodendron tulipifera* L.), black cherry (*Prunus serotina* Ehrh.), oak (*Quercus* spp.), sugar maple (*Acer saccharum* Marsh.), American beech (*Fagus grandifolia* Ehrh.), and white ash (*Fraxinus americana* L.). Evergreen forests are less extensive, primarily constrained to eastern hemlock (*Tsuga canadensis* (L.) Carrière) stands within riparian zones, and in the southern portions of the study area, which exhibit stands of loblolly pine (*Pinus taeda* L.) and Virginia pine (*Pinus virginiana* Mill.). Understory vegetation can be evergreen consisting of great laurel (*Rhododendron maximum* L.) and mountain laurel (*Kalmia latifolia* L.), the distribution of which is patchy and a function of the overstory canopy and topographic position (Chastain & Townsend, 2008). A number of understory invasive plants are present, particularly in forest edge habitat and small fragments of forest (Minor *et al.*, 2009). Several of the shrubs in this category have an early phenology more similar to cool season grasses than to native overstory trees (Wilfong *et al.*, 2009).

Data set description and pre-processing

The data used in this work were selected from all available Landsat Thematic Mapper (TM) and Enhanced Thematic Mapper plus (ETM+, SLC-ON) acquisitions for path 15/row 33 containing <20% cloud (Irish *et al.*, 2006). Using visual inspection, we further filtered these data and removed images containing semi-transparent clouds or substantial portions of surface ice and snow that we expected to be problematic. This resulted in a data set of 90 images of appropriate quality. The data were distributed roughly evenly across DOY, but were slightly biased towards the more recent decade (Fig. 1). All data were processed to standard terrain correction (Level 1T) radiometric and geometric accuracy by the USGS prior to our acquisition of the data (Woodcock *et al.*, 2008).

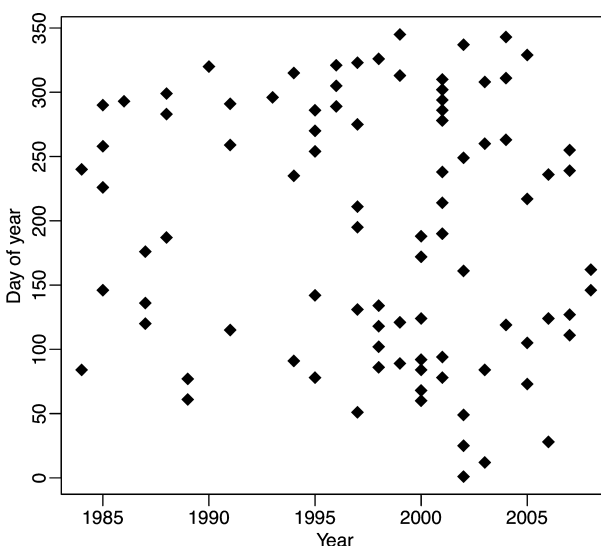


Fig. 1 The data used for this study encompassed 90 Landsat TM and ETM+ data acquisitions, spanning 25 years and the entire calendar year.

To account for variations in atmospheric scattering between scenes we performed a dark object subtraction, which removes the effects of path radiance. For each image, the darkest pixel was selected from a collection of deep lakes, and its spectrum was subtracted from that of all other pixels. No attempt was made to correct for differences in gain (atmospheric transitivity) between data sets as this correction is not necessary when performing change detection on multispectral remote sensing data (Song *et al.*, 2001). This decision is also justified by the relative insensitivity of the Landsat spectral bands to atmospheric water vapor and the strong contrast between spectra of vegetation (of primary interest here) and the spectra of other surfaces. Nevertheless, future work might consider employing a more comprehensive atmospheric correction procedure, such as offered by the Landsat Ecosystem Disturbance Adaptive Processing System (Masek *et al.*, 2006). Finally, a sun canopy sensor correction was performed to normalize for topographic effects and differences in sun zenith angle between data sets. This correction normalizes the radiance received from north and south facing slopes, as well as sun elevation changes through the year (Gu & Gillespie, 1998).

Spectral mixture analysis (SMA) (Adams *et al.*, 1986; Smith *et al.*, 1990; Elmore *et al.*, 2000) of every scene was performed using a common set of four image-derived endmember spectra representing photosynthetic vegetation (PV), non-photosynthetic vegetation, substrate (e.g. bare soil, impervious surfaces), and water/shade (represented by a spectrum acquired from a deep clear lake). Spectral mixture analysis assumes that each pixel is a linear combination of endmember spectra, each weighted by the fractional cover of that endmember. The forward equation and model assessment are embodied by the equations:

$$DN_b = \sum_{i=1}^N f_i DN_{i,b} + E_b \quad (1)$$

$$\text{RMSE}_{\text{SMA}} = \sqrt{\frac{\sum_{b=1}^B (E_b)^2}{B}} \quad (2)$$

where DN_b is the observed satellite response in wavelength, b ; $\text{DN}_{i,b}$ is the i^{th} image endmember response in band b , f_i is the fraction of the i^{th} endmember necessary to account for the observed response (DN_b), E_b is the residual response in band b in the same units as DN_b , N is the number of endmembers, and B is the number of wavelength bands used (6 in this application utilizing Landsat TM and ETM+ data). Equation (2) was used to summarize the model fit across all wavelength bands. Using linear model inversion techniques (Menke, 1989), we solved for the four endmember-fractions simultaneously. SMA has been shown to be a robust measure of greenness in a wide variety of ecosystems, notably exhibiting linearity with vegetation cover and insensitivity to background reflectance, including snow (Adams *et al.*, 1986; Smith *et al.*, 1990; Mustard, 1993; Elmore *et al.*, 2000; Asner *et al.*, 2003; Small, 2004). Although it is more common in phenology research (White *et al.*, 2009), the NDVI produces slightly lower values over snow compared with other types of substrate, thus delaying predictions of the onset of greenness (Fisher & Mustard, 2007).

Phenology curve fitting

The resulting timeseries of photosynthetic vegetation fraction (f_{PV}), stacked by DOY, reflects the average temporal pattern of leaf development, growing season stability, and senescence at any given location. An initial investigation of the data confirmed that a logistic sigmoid growth curve would be an appropriate model form to fit to spring and autumn trajectories in f_{PV} . The logistic curve has been used in numerous investigations of phenology, including our primary inspiration (Fisher *et al.*, 2006), but also the MODIS phenology product (Zhang *et al.*, 2003) and recent MODIS phenology validation projects (Liang *et al.*, 2011), to model increasing greenness in spring and decreasing greenness in autumn.

The usual form of the dual logistic curve is:

$$v(t, \mathbf{m}) = m_1 + m_2 \left(\frac{1}{1 + e^{m_3 - m_4 t}} - \frac{1}{1 + e^{m_5 - m_6 t}} \right) \quad (3)$$

where $v(t, \mathbf{m})$ is the modeled f_{PV} at time t (in DOY), and $\mathbf{m} = [m_1, m_2, m_3, m_4, m_5, m_6]^T$ where m_1 is the average f_{PV} measured in winter, m_2 is the difference between summer-time f_{PV} and m_1 , and $m_{3,4}$ and $m_{5,6}$ are parameters that adjust the shape of the sigmoid growth curve in spring and autumn, respectively. It has been shown how Eqn (3) can be fit to annual timeseries of vegetation greenness (Fisher *et al.*, 2006). The DOY where greenness is changing most rapidly (highest first derivative), is halfway between the winter minimum and summer maximum, and is calculated as m_3/m_4 (spring) and m_5/m_6 (autumn). These inflection points are termed the spring onset of greenness and autumn offset of greenness (*sensu* Fisher *et al.*, 2006).

Despite the simplicity and proven effectiveness of Eqn (3) for modeling phenological transitions in forests, we found that this equation often under-predicted observations in early sum-

mer and over-predicted observations in late summer due to declining greenness although the summer months (i.e. 'green-down' as discussed in the Introduction). This systematic discrepancy between observed and predicted data during the summer months suggested that the model in Eqn 3 is not capable of fully capturing the phenological dynamics, which might result in biased parameter estimates. To account for these summer trends in greenness, we constructed a new formulation of the standard logistic curve that utilized a sloped line to join the spring increasing curve and autumn decreasing curve. The addition of the summer greendown parameter [m_7 in Eqn (4), below] accomplished this goal. Additionally we made the following variable substitutions: $m_3' = m_3/m_4$, $m_4' = 1/m_4$, $m_5' = m_5/m_6$, $m_6' = 1/m_6$, resulting in a new formulation for $v(t, \mathbf{m})$,

$$v(t, \mathbf{m}) = m_1 + (m_2 - m_7 \cdot t) \left(\frac{1}{1 + e^{(m_3' - t)/m_4'}} - \frac{1}{1 + e^{(m_5' - t)/m_6'}} \right) \quad (4)$$

In this new formulation of the classic dual logistic curve, the spring onset and autumn offset of greenness are explicit model parameters (m_3' and m_5' , respectively) and the slope of the spring and autumn trajectories are the parameters m_4' and m_6' . In the original form (Eqn 3), the parameters determining the shape of the increasing and decreasing sigmoid functions, which also defined the spring onset and autumn offset, were strongly correlated, making unique predictions of these parameters problematic. The above variable substitutions greatly improve the ability to make unique estimates of spring and autumn timing in a relatively few number of iterations.

Inversion theory (Menke, 1989) offers elegant methods for calculating the nonlinear least-squares solution for the seven parameters in Eqn 4 given sufficient data on the f_{PV} throughout the year. This is accomplished by minimizing an objective function (ϕ) that contains a combined measure of data misfit (ϕ_d) and model length (ϕ_m).

$$\phi = \phi_d + \phi_m = \|\mathbf{W}_d(\mathbf{d}_{\text{obs}} - \mathbf{v}(t, \mathbf{m}))\|_2^2 + \|\mathbf{W}_m(\mathbf{m} - \mathbf{m}_{\text{ref}})\|_2^2 \quad (5)$$

In ϕ_d , \mathbf{d}_{obs} are the observed values of $v(t)$ at DOYs where there are data available; $\mathbf{v}(t, \mathbf{m})$ is the set of predicted data corresponding to model values $\mathbf{m} = [m_1, m_2, m_3', m_4', m_5', m_6', m_7]^T$ and at the observed times, t ; and \mathbf{W}_d is a diagonal matrix with elements $1/\sigma_i$, where σ_i is the expected error in the i^{th} measurement. In the model regularization term, ϕ_m , \mathbf{m}_{ref} is a reference model that is used to constrain the solution, and \mathbf{W}_m is the estimated model covariance matrix, which is a diagonal matrix with elements equal to the expected standard deviations in model parameters. The estimated parameter uncertainties in \mathbf{W}_m are chosen to be relatively broad so that they do not overly constrain the solution, but provide necessary stability in the inverse problem.

The model regularization term (ϕ_m) serves two primary roles in the estimation of parameter values. First, due to the fact that typical parameter values vary over several orders of magnitude (10^2 for m_3' and m_5' to 10^{-4} for m_7), there is significant variability in the sensitivity of the model to each parameter. By including appropriate values in \mathbf{W}_m , parameters with relatively low sensitivities can be more accurately estimated in the inverse solution. Second, numerical instabilities can occur

in the solution of the inverse problem due to the nonlinearities in Eqn (4) that, without the regularization term, result in an ill-posed set of equations.

The solution to the nonlinear inverse problem that minimizes Eqn (5) involves iteratively solving for perturbations to the model parameters ($\delta\mathbf{m}$), starting from an initial estimate, \mathbf{m}_0 . The equation for model updates is given by

$$\delta\mathbf{m}_i = [\mathbf{G}^T \mathbf{W}_d^T \mathbf{W}_d \mathbf{G} + \mathbf{W}_m^T \mathbf{W}_m]^{-1} [\mathbf{G}^T \mathbf{W}_d^T \mathbf{W}_d (\mathbf{d}_{\text{obs}} - \mathbf{v}(t, \mathbf{m}_{i-1})) + \mathbf{W}_m^T \mathbf{W}_m (\mathbf{m}_{\text{ref}} - \mathbf{m}_{i-1})] \quad (6)$$

Updates to the current model are calculated as $\mathbf{m}_i = \mathbf{m}_{i-1} + \delta\mathbf{m}_i$, and the iterative process is continued until a desired level of data misfit is achieved (more specifics below). \mathbf{G} is the matrix of partial derivatives (i.e. the Jacobian matrix) of Eqn (4), with each column equal to the partial derivative of $v(t, \mathbf{m})$ with respect to a different parameter and rows corresponding to the DOYs for which data are available. In our case \mathbf{G} was a 90×7 matrix, given 90 data points and 7 parameters. Because \mathbf{G} is a function of the model parameters, it is recalculated at each step of the nonlinear inversion with respect to the current model estimate, \mathbf{m}_{i-1} . The reference and first estimate of model parameters (\mathbf{m}_{ref} and \mathbf{m}_0 , respectively) were chosen close to the expected scene-wide mean value: $\mathbf{m}_{\text{ref}} = \mathbf{m}_0 = [0.07, 1.3, 125, 7, 300, 7, 0.003]$. Although these values are important to model performance, the global minimum of Eqn 5 can be attained as long as \mathbf{m}_{ref} and \mathbf{m}_0 are chosen such that the expected true model parameters fall roughly within two standard deviations of the chosen reference model.

Specification of the *a priori* information on parameter standard deviations and data errors (\mathbf{W}_m and \mathbf{W}_d , respectively) provides important controls on the solution of the inverse problem. We estimated prior standard deviations on model parameters as $[0.05, 0.5, 30, 2, 30, 2, 0.002]$. These values gave sufficient flexibility to the model parameters so that the model arrived at a solution in a small number of iterations (<5), greatly improving computational speed compared with using smaller *a priori* parameter variances. Assigning a very small variance to a particular model parameter has the effect of biasing that parameter towards the reference model value, regardless of the effect on the data fit. Thus, by setting the *a priori* variance for m_7 to an extremely small value, and $m_{\text{ref},7} = 0$, the solution is strongly constrained to have $m_7 = 0$, thus defaulting to a version similar to Eqn (3). This provides a useful way to assess model improvement with the inclusion of the green-down parameter, and study changes in the resulting estimates for spring and autumn phenology.

Large *a priori* estimates of data errors (small values on the diagonals of \mathbf{W}_d) down-weight the importance of fitting the data compared to satisfying the model regularization constraints. Our estimates of *a priori* data variances were derived from studies that have compared SMA-derived estimates of f_{PV} to field measured values. Elmore *et al.* (2000) completed a rigorous analysis of uncertainty in a semi-arid environment and determined that errors were Gaussian, independent of time, and approximated one standard deviation uncertainties at 0.04. Other studies in forested systems have produced similar results (Lobell *et al.*, 2001). From these studies we decided

that 0.05 was an appropriate, conservative, value for the *a priori* estimates of data errors. Because \mathbf{W}_d is an *a priori* estimate, it does not take into account spatial variation or the outlier status of data uncertainties.

The L1 norm and minimizing the effect of outliers

Outlier management is a reoccurring problem when attempting to measure phenologically important dates from remote sensing time series. Typical solutions to the problem of outliers include using composite data generated from the best observation in each 8- or 16-day window (Zhang *et al.*, 2003), the application of timeseries filtering or smoothing functions (Bradley *et al.*, 2007; Tuanmu *et al.*, 2010), or utilizing a non-uniform data-weighting matrix where *a priori* data variances are estimated from the RMSE_{SMA} (Fisher *et al.*, 2006). We investigated several of these options but found that data residuals were non-gaussian, suggesting diverse sources of error that were not well correlated with available *a priori* estimates of data error (e.g. RMSE_{SMA}, thermal anomalies due to cloud and snow, or estimates of atmospheric scattering). We found that outliers were inconsistently due to any of these processes, depending on the time of year, yet were sometimes due to actual changes in the surface such as changes in land use.

An elegant solution to problems of this nature is to minimize the L₁ norm of the data misfit, rather than the L₂ norm that was specified in Eqn (5). This identifies the median fit to the data instead of the mean fit by minimizing the absolute data residuals rather than the squared residuals. Minimization of the L₁ norm reduces the penalty on outliers, which helps to avoid model errors caused by over-fitting bad data points. This technique introduces additional nonlinearity into the inverse problem, but is easily implemented by iteratively re-weighting data weights based on the absolute residual data variance (Scales *et al.*, 1988). Here, the data residuals calculated after each iteration are placed on the diagonals of a re-weighting diagonal matrix, \mathbf{R} , which is used to scale the data weights for the subsequent model update (Farquharson & Oldenburg, 1998), so that Eqn (6) becomes:

$$\delta\mathbf{m}_i = [\mathbf{G}^T \mathbf{W}_d^T \mathbf{R} \mathbf{W}_d \mathbf{G} + \mathbf{W}_m^T \mathbf{W}_m]^{-1} [\mathbf{G}^T \mathbf{W}_d^T \mathbf{R} \mathbf{W}_d (\mathbf{d}_{\text{obs}} - \mathbf{v}(t, \mathbf{m}_{i-1})) + \mathbf{W}_m^T \mathbf{W}_m (\mathbf{m}_{\text{ref}} - \mathbf{m}_{i-1})] \quad (7)$$

Note that the original prior estimates of data uncertainty encompassed in \mathbf{W}_d are still included, but are modified by the absolute data residuals following each iteration. Solutions calculated from Eqn 7 are robust in their insensitivity to outliers, which has many desirable qualities. Most notably, land-use or climate-driven changes in phenology that might have occurred near the end of the Landsat era and thus appear as timeseries outliers, have minimal impact on the calculation of the parameters using Eqn (7).

Equation (7) was solved until the L₁ norm of the model misfit (a unitless measure equal to the sum of the weighted data residuals), given by

$$\text{Misfit} = \sum_1^N |\mathbf{W}_d d_{\text{res}}| \quad (8)$$

reached a target value. The L_1 norm sums the data residuals weighted by the *a priori* data weights, and therefore is dependent on the number of observations (in this case, $N = 90$). The appropriate target value for the L_1 -norm model misfit was chosen to be

$$\phi_d^{\text{tar}}(L_1) = N\sqrt{2/\pi} = 71.8 \quad (9)$$

based on previous work (Parker & McNutt, 1980). To avoid situations where $\phi_d^{\text{tar}}(L_1)$ is never reached, the inversion is stopped when additional iterations reduce $\phi_d(L_1)$ by <0.5% [i.e. stop when $(\phi_d(L_1)_i - \phi_d(L_1)_{i-1})/\phi_d(L_1)_{i-1}$], or when the number of iterations for any pixel reaches 100. When this latter constraint was actually reached, pixels were flagged as unreliable and ignored in further analyses.

Estimates of model parameter uncertainty

We used Monte Carlo bootstrapping methods (Efron, 1979; Efron & Tibshirani, 1991) to estimate parameter uncertainties for a selection of 50 pixels spanning a gradient in elevation across the Blue Ridge Mountains. For each pixel, we re-sampled the original data set, d_{obs} , with randomly chosen data points removed and replaced by duplicating existing samples. In this work, 5000 re-sampled data sets were generated and inverted for the seven unknown parameters using Eqn (7) at each pixel. In a second set of bootstrap models, we constrained the *a priori* variance for m_7 and $m_{\text{ref},7}$ to equal 0, and thus enabled a comparison of model performance with and without the greendown parameter (m_7). The distribution of parameter estimates for these bootstrap models provides valuable information about parameter uncertainty and correlation that is free of assumptions about the underlying data distributions.

Classification of forest pixels

We chose to focus on forest trees. Forests are the native land cover of the mid-Atlantic, and although cool season grasslands (pasture, hay, and lawn) are as common, their land surface phenology as viewed by Landsat sensors are more likely than forest trees to be impacted by management styles that vary annually (Asner *et al.*, 2004; Elmore & Craine, 2011). At the 30-m pixel size, mixed pixels are common, but many pure forested pixels exist in a wide range of landscapes, from urban to rural. Therefore, by performing a per-pixel classification of forests, we expected to enable an analysis of forest phenology across the entire study area, despite significant forest fragmentation. Previous studies at this spatial resolution were conducted in New England, USA and made the distinction between deciduous and evergreen forests (Fisher *et al.*, 2006). Here we chose a definition of forest that included both deciduous and evergreen trees because in the mid-Atlantic, evergreen trees represent a smaller portion of the landscape and, regardless, our initial observations revealed that Eqn 4 was accurately fitting leaf area changes from evergreen canopies.

We classified forest pixels using a maximum likelihood supervised classification scheme on the resulting parameter set. Training areas were digitized from eight aerial photo-

graphs available for the study region via the National Agriculture Imagery Program (NAIP) from 2003. The areas selected for training were all closed canopy forests and spanned the entire study area including all physiographic provinces. In the classification we included all parameters (7) and the misfit [Eqn (8), which was lower for forest pixels], for a total of eight variables. The inclusion of the data misfit had the desirable effect of excluding pixels that were not fit well by the model, most likely due to land use changes occurring during the Landsat era. The resulting classification resulted in 11.5 million forest pixels, which was 39% of terrestrial image area. We visually inspected the resulting classification and noted that it appeared to represent forest area conservatively, but performed no rigorous classification validation. Misclassified pixels appear as noise in subsequent analyses of the effect of landscape variables.

Understanding and using model parameters

Equation 4, with the fitted parameters, describes the leaf development, summer stability, and autumn senescence of forested canopies. To explore the multicollinearity between phenological information and key vegetation cover values we calculated Pearson correlation coefficients between each pair of parameters extracted directly from Eqn (4), with the replacement of m_2 with maximum vegetation cover (MAX-VEG). MAXVEG is not equal to $m_1 + m_2$ except in rare cases where m_7 equals zero. Thus, we calculated MAXVEG as the maximum of Eqn (4) using the final parameter set for each pixel.

Comparison with daily webcam data

We utilized a webcam mounted above a forest canopy to quantify, at high temporal resolution, seasonal changes in the optical properties of a forest canopy. These data offer an excellent platform for comparing remote sensing-based and ground-based phenology observations, due to their intermediate scale and, thus, comparability with these two endmember approaches. Recent studies (e.g. Richardson *et al.*, 2007; Ahrends *et al.*, 2008) have demonstrated how camera imagery can be used to quantitatively monitor both seasonal development and senescence of deciduous broadleaf forest canopies and even seasonal changes in the apparent 'greenness' of evergreen conifer canopies. With three channels (colors) of information, webcams provide insight into not only the amount of foliage present (e.g. estimates of leaf area index), but also its physiological capacity for photosynthesis (Richardson *et al.*, 2009a; Richardson *et al.*, 2009b).

Across the eastern US and Canada, the PhenoCam network (<http://phenocam.sr.unh.edu/>) comprises roughly 80 sites where digital webcams are recording daily (or in some cases hourly) images of forest vegetation. We identified the only webcam within our study region, maintained by the National Park Service and located adjacent to the national capitol building. Within this camera's field of view, we identified a large stand of closed-canopy deciduous forest and sampled the green and red intensity measured by the camera at daily intervals (at local noon) for the available period, 2004–2008. Several

metrics of greenness have been developed for analyzing webcam data. We chose one that mimics the NDVI, thus normalizing for variation in overall image intensity. We calculated $\text{WebCam}_{\text{veg}}$ using the following equation (Brügger *et al.*, 2007):

$$\text{WebCam}_{\text{veg}} = \frac{\text{DN}_{\text{green}} - \text{DN}_{\text{red}}}{\text{DN}_{\text{green}} + \text{DN}_{\text{red}}} \quad (10)$$

where DN_{red} and DN_{green} are camera's response in the visible red and green, respectively. We then located and sampled the four Landsat pixels that corresponded to the forested stand apparent in the webcam image (located at latitude 38.888°N and longitude 77.062°W). After confirming that all four pixels were roughly identical and all located in closed canopy forest, we calculated the mean f_{VEG} and parameter values, thus generating a single f_{VEG} timeseries and corresponding phenology curve. Several important landmarks (e.g. the Washington Monument) were apparent in the image, thus guaranteeing a close match between the webcam field of view and the Landsat pixels sampled. However, the angle of observation was considerably different with the webcam observation angle approximately 60 degrees off nadir.

We fit the phenology curve (Eqn 4) to the webcam data for each year individually (4 years of data) and the average annual curve (generated by averaging by DOY). These results were quantitatively compared against the average Landsat phenology curve.

Comparison with autumn aerial photography

Fisher *et al.* (2006) extensively validated the date of the onset of greenness resulting from a curve-fitting technique that was similar to the technique described here. More recent attempts to validate satellite-based phenology observations have been equally successful and support the use of logistic curve modeling, particularly for the spring onset of greenness (Liang *et al.*, 2011). Therefore, we concentrated our validation efforts on autumn phenology using aerial photography that was collected during leaf senescence from a single year. We identified a region with topographic relief sufficient to offer a variety of autumn leaf color and available high-resolution aerial photography approximately 15 km south of Harpers Ferry, WV. Color aerial photography was acquired from the National Map seamless data server for the month of October 2008 with 0.3-m pixel resolution.

From this October aerial photograph, we sought to compare autumn coloration with the date of autumn offset of greenness. This required using a method different from that used to analyze the webcam data, which only quantified the contrast between the visible green and red wavelengths. We expected more green hues to be present in pixels returning a latter autumn offset and more red and yellow hues (depending on the dominate tree species) to be present in pixels returning an earlier autumn offset. After evaluating different options for extracting color information from three-band visible color photography, we selected a hue-intensity-saturation (HIS) transformation (Wang *et al.*, 2005) using the ENVI image processing software package (ITT Visual Information Solutions).

The resulting hue vector was compared with the original red-green-blue image and it was determined that hue values between 0–90 corresponded to yellow, 90–180 to green, 270–360 to red, and 180–270 to blue (Naik & Murthy, 2003). We utilized a simple decision tree to classify the hue using each of these ranges corresponding with a visible color. Atmospheric scattering, which is strongest at blue wavelengths, resulted in the appearance of a blue hue within all shadowed pixels. Therefore, all pixels classified as blue using the above data ranges were labeled as no data and made transparent in finished maps.

Investigating landscape patterns

To enable an evaluation of landscape controls on phenology, we generated maps at 30-m resolution for five different parameters: elevation, aspect, distance to tidal water, impervious surface area (ISA), and latitude. These parameters were chosen because of their expected impact on local climate and photoperiod, both known to influence forest phenology (see references in the Introduction). National Elevation Data (30 m NED) was acquired from the USGS seamless data server. From these data, aspect was calculated as the angular (degrees) displacement from north, and therefore ranged between 0 and 180 degrees. Although there might be potentially important differences in forest phenology between East and West facing slopes, we could not find any evidence for this effect; therefore, East and West facing slopes received the same value of 90 degrees. A map of tidal water was derived from a coastline map and the distance from tidal water was calculated for each 30-m pixel using the ESRI ArcGIS software package. Finally, the 2001 National Land Cover Data ISA data layer was acquired from the USGS seamless data server and a 5×5 pixel spatial mean filter was applied. The filter replaces the center pixel in each 5×5 pixel box with the mean ISA of the 25 pixels in the box. Therefore, a 30-m forest pixel surrounded by development resulted in a higher mean ISA value than a forest pixel surrounded by forest. We also generated a map of distance to the geographic centers of the cities of Baltimore and Washington, DC.

We viewed the entire data set of 11 million forest pixels as too large for efficient analysis. Additionally, for multiple regression analysis using nearly continuous spatial data, spatial autocorrelation causes adjacent pixels to be very similar and therefore the inclusion of such pixels is essentially the same as duplicating data points. Therefore, we reduced the total data set by arranging a grid of points with 500-m spacing in both the X and Y direction. If a point did not fall on a forest pixel it was deleted from the database, otherwise it was included. The resulting set of sample points totaled 29 819 data, 14 110 in the Coastal Plain, 13 263 in the Piedmont plateau, and 2446 in the Blue Ridge. At each location we sampled the four landscape variables mentioned above, along with the X and Y position, expressed in meters in UTM projection, zone 18. We then divided the data set into three parts, one for each physiographic province to explore the relative importance of landscape variables between provinces.

Using these three data sets we constructed multiple linear regressions (Type III) for each physiographic province using all landscape factors as model effects, and the date of spring onset of greenness, the date of the autumn offset of greenness, and growing season length as model responses. Despite 500-m spacing between data points, we expected spatial autocorrelation to increase the significance of landscape variables. To account for this, we calculated a cubic trend surface by including all third-degree polynomial terms of the X and Y position of the sample locations (Lichstein *et al.*, 2002). As an example, the model exploring the effect of landscape variables and landscape position on the onset of greenness in the Piedmont plateau was:

$$\begin{aligned}
 m_{3,PP} \sim & b_0 + b_1^* \text{Elevation} + b_2^* \text{Aspect} \\
 & + b_3^* D_{\text{tidal}} + b_4^* \text{ISA} + b_5^* Y + b_6^* X + b_7^* XY + b_8^* X^2 \\
 & + b_9^* Y^2 + b_{10}^* X^3 + b_{11}^* Y^3 + b_{12}^* X^2 Y + b_{13}^* XY^2 + \varepsilon_r
 \end{aligned} \quad (11).$$

The term representing the Y position (latitude) is the only spatial term that is expected to directly influence phenology. All the other spatial terms (combined) are included to reduce the effect of spatial autocorrelation on the significance of the other model effects. By including the cubic trend surface we also enabled an analysis of the spatial structure unaccounted for by the landscape variables included in the model. For each regression, we calculated model estimates and the fraction of the sum of squared variance each model estimate explains in the overall regression. A P -value (probability of significance) was calculated for each model effect.

Results

Parameter uncertainty

The 7-parameter model exhibited a visually improved data fit compared with the 6-parameter model, which lead to several quantitative improvements in terms of data residuals, the dependence of the autumn offset of greenness on summer greendown, and model parameter uncertainties. For the 50 pixels included in the Blue Ridge and piedmont test data set, the misfit (Eqn 8) decreased an average of 15.5% with the inclusion of the 7th parameter, but the largest improvement occurred in the temporal balance of the residuals. For the 6-parameter model, data residuals were positive between DOY 120 and 210 and negative between DOY 210 and 300. However, the 7-parameter data residuals through this period were much closer to zero and did not appear to be either more positive or more negative in either early summer or late summer (Fig. 2). This reduction in 'structure' within the residuals is a strong indicator that the 7-parameter model more accurately captures the phenological dynamics than the 6-parameter model.

The 7-parameter model always predicted a later spring onset and autumn offset of greenness than the 6-parameter model, but for the autumn offset the differ-

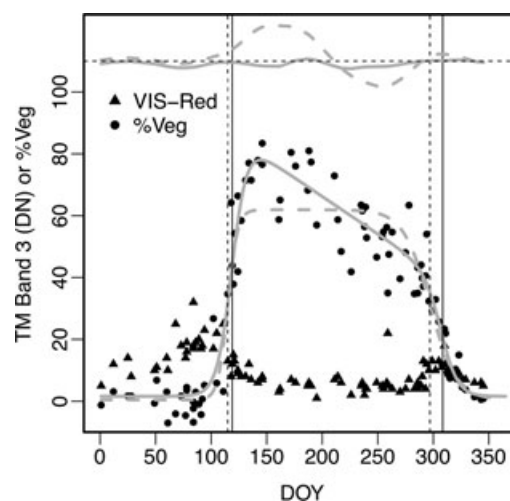


Fig. 2 Landsat%Veg annual trajectories of spring onset, summer stability, and autumn offset of greenness (\bullet) modeled using the 6-parameter (dashed line) and 7-parameter (solid line) equations for a deciduous forest pixel. The model residual is plotted as a smoothed function of DOY along the top of the figure, showing smaller and more uniform residuals for the 7-parameter model. Autumn color [shown using the visible red (Landsat band 3; \blacktriangle)] increases just prior to the inflection point of the descending sigmoid curve (vertical lines).

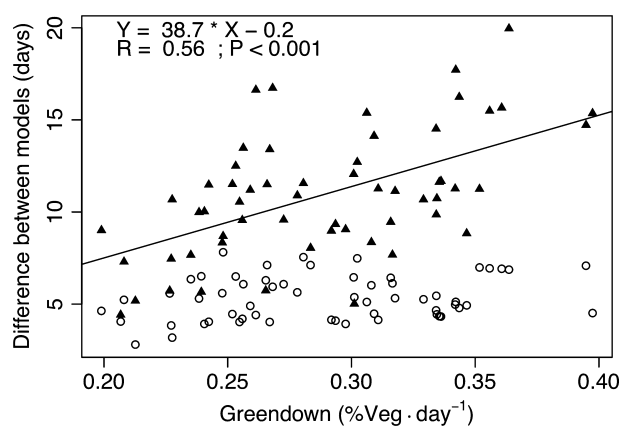


Fig. 3 The difference between the spring onset (\circ) and autumn offset of greenness (\blacktriangle) as predicted by the 6- and 7-parameter models plotted against summer greendown as measured by the 7-parameter model. The 7-parameter model always predicts a later spring onset and autumn offset, but the difference is greater for the autumn offset, resulting in a longer growing season prediction, particularly for pixels with a strong greendown.

ence was greater and depended strongly on summer greendown (Fig. 3). The later phenology in spring is a consequence of higher maximum vegetation cover in spring, which delays the spring inflection point by an average of 5 days. In autumn, the 6-parameter model

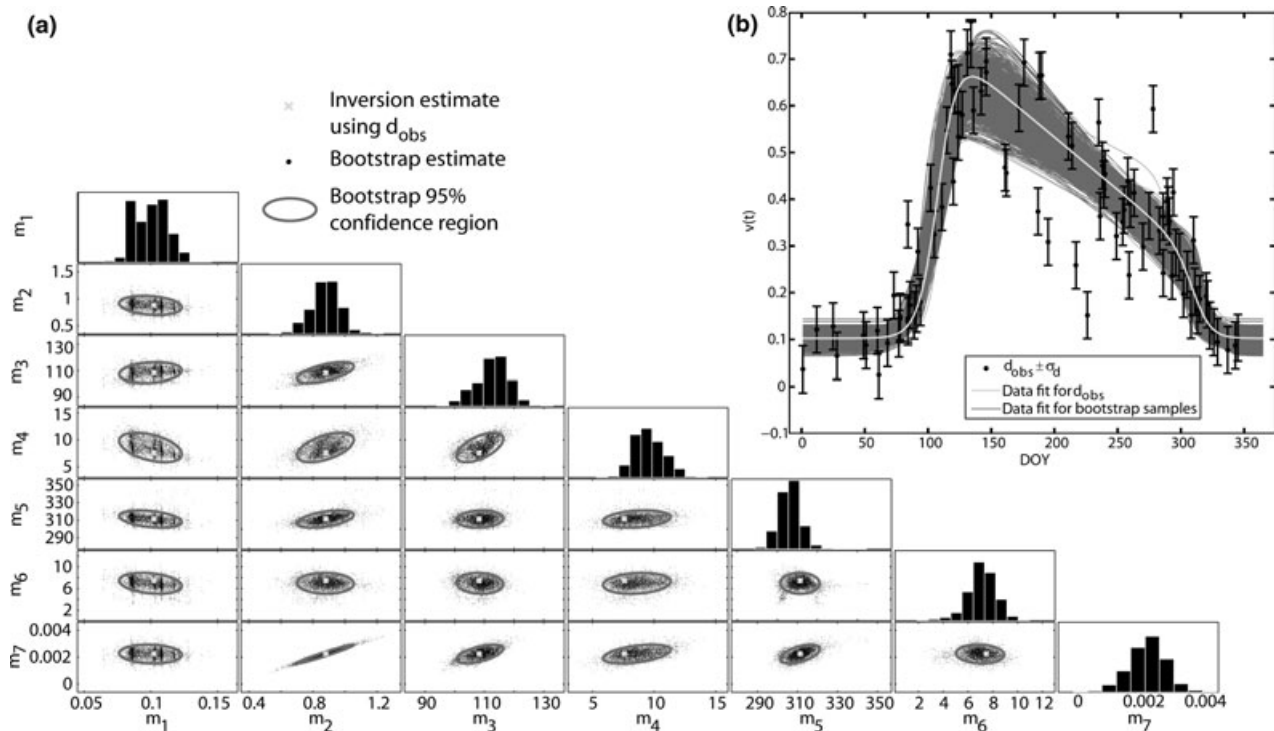


Fig. 4 (a) Summary of bootstrapping results on a single pixel. Diagonal elements show histograms of all 5000 bootstrap estimates for each parameter, and off-diagonals show crossplots of all parameter combinations, providing details about parameter correlation. Parameter estimates using the full d_{obs} (gray x) and the bootstrap 95% confidence region (ovals) are also shown. (b) Original data with error bars (black), the data fit for the inversion result using d_{obs} (gray), and the data fits for the bootstrap samples (dark gray).

Table 1 Summary of bootstrapping results

| Parameter | Meaning | Inversion estimate using d_{obs} | Mean bootstrap estimate | Bootstrap 95% lower bound | Bootstrap 95% upper bound |
|-----------|----------------------------|---|-------------------------|---------------------------|---------------------------|
| m_1 | Minimum vegetation cover | 0.1023 | 0.9977 | 0.08046 | 0.1210 |
| m_2 | Potential amplitude | 0.8802 | 0.8779 | 0.6917 | 1.042 |
| m_3' | Spring onset of greenness | 108.2 | 108.5 | 100.0 | 115.7 |
| m_4' | Slope of spring onset | 7.596 | 8.600 | 6.182 | 11.45 |
| m_5' | Autumn offset of greenness | 311.4 | 311.4 | 301.6 | 321.5 |
| m_6' | Slope of autumn offset | 7.473 | 6.971 | 4.657 | 8.742 |
| m_7 | Summer greendown | 0.002250 | 0.002231 | 0.001499 | 0.002898 |

over predicts late summer greenness, which forces the model to predict an earlier autumn to maximize model fit through the period of leaf senescence. This effect is strongest in the late summer, influencing the estimates of the beginning of autumn most, and decreases into the late autumn. Pixels with a stronger summer greendown exhibited a larger difference between models' prediction of autumn phenology, ranging from 7 to 20 days (Fig. 3). The dependence of autumn phenology on summer greendown is therefore removed by utilizing the 7-parameter model.

The bootstrapping results show only a moderate deviation from normality in the distribution of parameter estimates (Fig. 4). Because the bootstrap distributions are approximately symmetric about the mean estimate, we report values with 95% confidence limits defined as half the difference between the upper and lower bootstrap bounds (Table 1). Doing so, the average uncertainty in the prediction of the autumn offset decreased nominally from ± 7.9 to ± 7.4 days and the maximum uncertainty decreased from 14.9 to 11.6 with the inclusion of parameter m_7 . We observe that there is

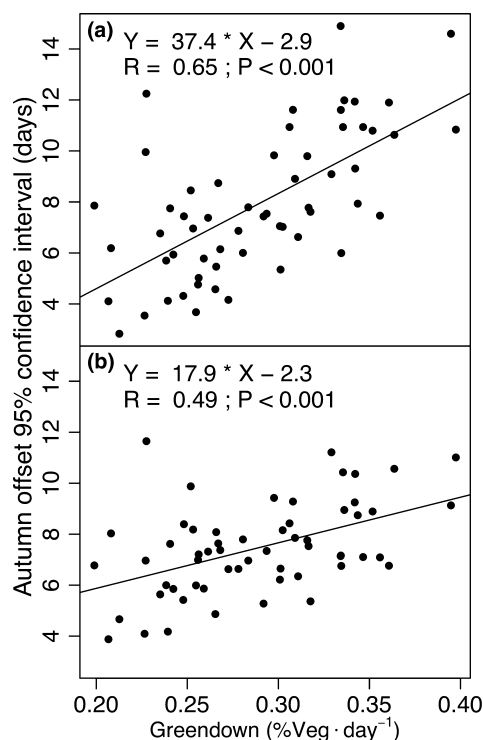


Fig. 5 The autumn offset 95% confidence interval (in days) for the 6-parameter model (a) and the 7-parameter model (b), both plotted against greendown calculated using the 7-parameter model. The models exhibit a similar range in uncertainty, but the relationship between the autumn offset uncertainty and greendown is reduced in the 7-parameter model.

a varying degree of correlation between parameters; for example, m_2 and m_7 are highly correlated, whereas m_3' and m_5' are uncorrelated. More important than average uncertainties, we found that the dependence of the autumn offset uncertainty on greendown in the case of the 6-parameter model was a factor of two larger than in the case of the 7-parameter model (Fig. 5). The 6-parameter model is, therefore, biased towards an early prediction of the autumn offset of greenness, the size of this bias is dependent on the strength of the summer greendown (Fig. 3), and uncertainty in the autumn offset prediction is dependent on the strength of the summer greendown (Fig. 5).

When applied to the entire data set, the model successfully returned a complete set of parameters for 99% of the image pixels. The distribution of misfit values peaked at 90, with a long thin tail towards larger values. In 33% of the cases, the optimum misfit (70) was reached and 99% of the forested pixels reached either the target misfit or the optimal misfit interval within 10 iterations. Forest pixels generally were modeled in five to six iterations whereas non-forest land covers generally took more iteration and returned a higher misfit.

Validation with high-resolution data

We validated the effectiveness of our method at small spatial scales using an aerial photograph acquired above the Blue Ridge Mountains, just south of Harpers Ferry, WV on 15 October 2008. For this mid-autumn image, red canopy hues spatially correlated with early autumn offset dates, yellow hues correlated with intermediate autumn offset dates, and green hues correlated with late autumn offset dates (Fig. 6). These patterns held up across scales, with patches of visually homogeneous color 5–10 Landsat pixels in size returning similar values. Representative of very fine scales, the webcam located in Washington, DC, showed good correlation with the average phenology derived from Landsat (Fig. 7). The webcam data exhibited summer green-down in all years of a similar intensity to that observed in the Landsat data.

Landscape patterns at large spatial scales

We calculated Pearson correlation coefficients between important phenological dates and vegetation cover estimates throughout the timeseries (Table 2). Some notable characteristics of the data set that are apparent from this analysis include:

- 1 The spring onset and autumn offset of greenness were negatively correlated, but not strongly ($r = -0.45$), suggesting that there are both similarities and differences between the set of environmental drivers that determine the timing of spring and autumn. This correlation is not predicted based on model structure (i.e. m_3' and m_5' are not correlated in Fig. 4). On the other hand, a theoretical perfect correlation between spring onset and autumn offset, using the bootstrapped uncertainties for each parameter (Table 1), leads to a correlation of -0.74 , significantly greater than the observed correlation. Despite this degree of independence between the timing of the spring onset and autumn offset, across the study region, variance in the spring onset ($\sigma^2 = 21.7$) and autumn offset ($\sigma^2 = 29.9$) are roughly equal. This indicates that neither dominates the variation in growing season length, particularly considering the larger uncertainty in the autumn offset compared with the spring onset, which leads to a higher variance.
- 2 Increasing greendown was associated with increasing MAX_{VEG} and a later spring onset. This suggests that forest canopies with high leaf area in spring greenup later and are more susceptible to summer green-down. Conversely, canopies that exhibit stable summer greenness (low greendown) are associated

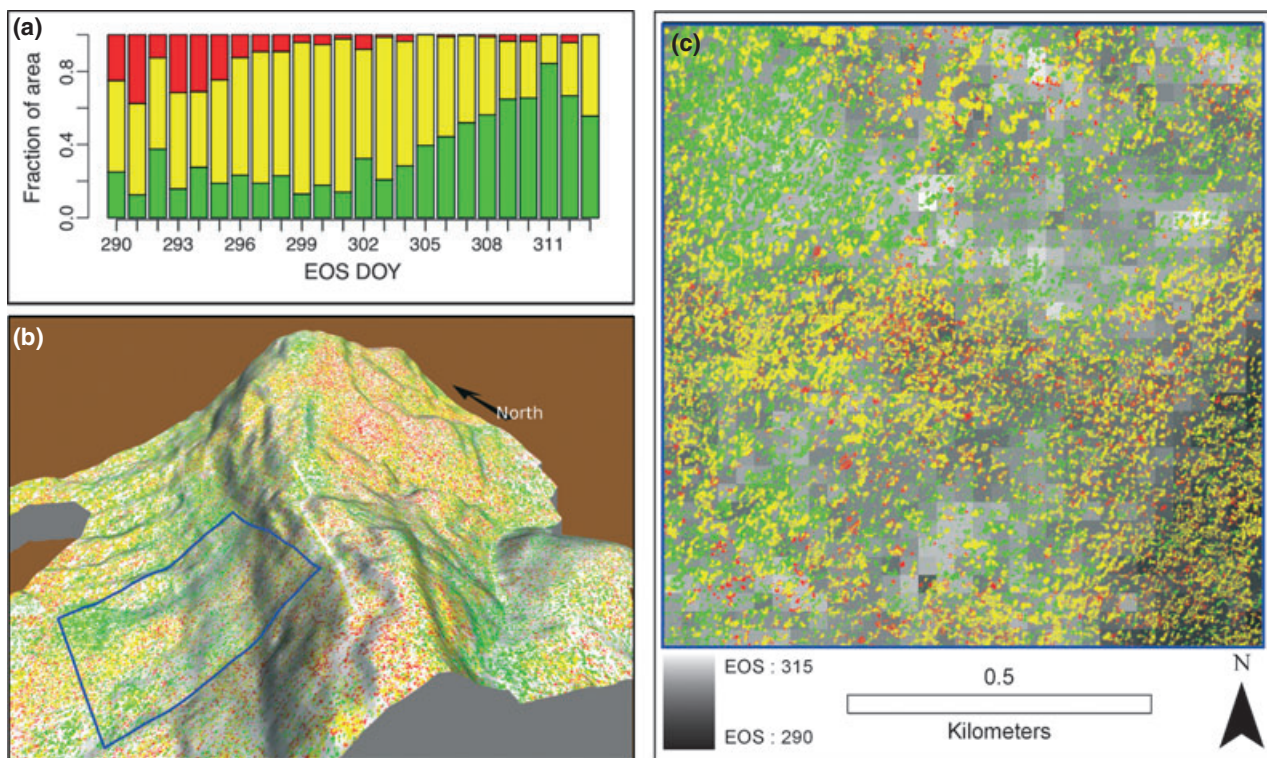


Fig. 6 Validation of the autumn offset was completed using an aerial photograph acquired on 14 October 2008 over the Blue Ridge Mountains, 15 km south of Harpers Ferry, WV. Sunlit canopies were classified as red, yellow, or green, discarding shadowed canopies (see text). The fractional area of each classified color was plotted against the date of autumn offset (end of season, EOS) calculated using the 7-parameter phenology model (a) showing that earlier autumn offset is related to red and yellow canopies and later autumn offset is related to green canopies in this autumn photograph. The spatial pattern of red, yellow and green canopies exhibits the influence of elevation, but also smaller scale variations that are likely micro-habitats supporting color-distinct species. Colors in b are draped over a hillshade image with the sun at 200 degrees azimuth and 40 degrees elevation.

with lower maximum vegetation cover and an earlier spring onset of greenness. However, one must be careful in interpreting this result because the bootstrapped model parameters also exhibited a strong correlation between m_2 and greendown (Fig. 4), suggesting the model structure strongly influences these relationships across pixels.

3. The slope of the spring and autumn transitions was not strongly correlated with any parameter. They were, however, weakly correlated with each other indicating that canopies that develop over a more extended period throughout the spring also take longer to senesce in the autumn. This relationship (unlike the relationship between MAX_{VEG} and greendown) was not seen in the bootstrapped model parameters, suggesting that it is not due to model structure. There was a weak negative correlation between the slope of the spring and autumn transitions and MAX_{VEG} (-0.22 and -0.23 , respectively) suggesting that forest canopies with low canopy cover in early summer achieve this state only slightly more rapidly than canopies with higher cover.

Elevation, distance to tidal water, impervious surface area, and latitude all significantly influenced the timing of spring onset and autumn offset of greenness, and therefore growing season length (Fig. 8). Aspect was not generally significant. For each significant landscape variable (elevation, tidal distance, urbanization, and latitude) the predicted relationship was stronger for the spring onset than for the autumn offset of greenness. Because the uncertainty in the autumn offset is 6 days larger than the uncertainty in spring onset (Table 1), it is possible that the more significant relationships found with spring timing is simply due to greater measurement precision. The importance of each of the four landscape variables varied across the three physiographic provinces (Table 3):

- 1 *In the Blue Ridge Mountains*, elevation accounted for 95% of the model variance in spring onset and growing season length, driving a highly predictive model for spring onset ($r^2 = 0.74$). However, elevation was less important in modeling the autumn offset and lead to a weaker model ($r^2 = 0.18$). The relationships

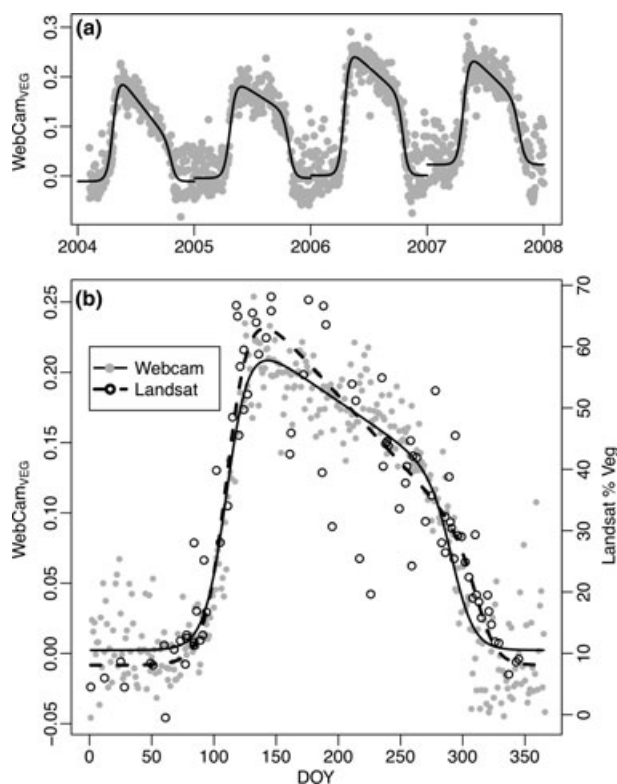


Fig. 7 (a) Four years of vegetation index measured daily from webcam imagery of canopy trees adjacent to the US Capital building, Washington, DC. In (b), the four years of webcam data have been averaged by DOY and plotted with the %Vegetation from Landsat with their respective 7-parameter phenology models.

between the spring onset and autumn offset and elevation were nonlinear, with increasing elevation associated with an *increasing* growing season length (earlier spring and later autumn) until an elevation of 275 m. Above this elevation, increasing elevation caused growing season length to decrease more rapidly (~4 days per 100 m). The reduction in growing season length observed with increasing elevation

above 250 m was driven to a greater extent by a later spring than by an earlier autumn (Fig. 9).

- 2 *In the Piedmont Plateau*, where extensive urban development has occurred, %ISA was generally the strongest model effect. We found that the effect of urban land cover extended out 32 km from city centers at which point a breakpoint occurred and further variation with urban distance approximated zero (Fig. 10). The effect of %ISA on autumn offset was greater than it was on the spring onset. In general data from the Piedmont Plateau did not result in strong explanatory models with r^2 values ranging from 0.11 to 0.22.
- 3 *In the Coastal Plain*, distance to tidal water was the most important predictor of both spring onset and autumn offset of greenness, explaining approximately 60% of model variance. Of secondary importance, was %ISA, which (similar to the Piedmont Plateau) explained more of the variance in autumn offset than spring onset. In general, the model effects used did not result in highly explanatory models, with r^2 values ranging from 0.09 to 0.12.

Spatial patterns evident from multiple linear regressions utilizing the entire data set held up at smaller spatial scales (Fig. 8a). In particular, elevation was correlated with the date of spring onset resulting in longer growing seasons. The small mountain shown in Fig. 8 exhibited longer growing seasons at all toe slopes and a shorter growing season at the summit. Fine-scale variability is also apparent, which has a spatial structure suggestive of variation in edaphic factors and plant community composition.

Discussion

Summer greendown has received inconsistent treatment in the remote sensing literature and is not accounted for at all in analyses of moderate to low resolution data (White *et al.*, 2009), influencing the calculation of autumn phenology dates (Friedl *et al.*, 2010; Ganguly *et al.*, 2010). Beginning in the 1990s, several papers reported that increasing leaf lifespan was

Table 2 Pearson correlation coefficients between phenologically important dates and quantities

| | | m_3' | m_5' | $m_5'-m_3'$ | m_4' | m_6' | m_7 | MAX _{VEG} | m_1 |
|--------------------|----------------------------|--------|--------|-------------|--------|--------|-------|--------------------|-------|
| m_3' | Spring onset of Greenness | 1.00 | -0.45 | -0.82 | -0.05 | -0.18 | 0.46 | 0.16 | -0.18 |
| m_5' | Autumn offset of greenness | -0.45 | 1.00 | 0.88 | 0.01 | 0.08 | -0.18 | -0.09 | 0.04 |
| $m_5'-m_3'$ | Growing season length | -0.82 | 0.88 | 1.00 | 0.03 | 0.15 | -0.36 | -0.14 | 0.12 |
| m_4' | Slope of spring onset | -0.05 | 0.01 | 0.03 | 1.00 | 0.34 | 0.21 | -0.22 | 0.01 |
| m_6' | Slope of autumn offset | -0.18 | 0.08 | 0.15 | 0.34 | 1.00 | -0.21 | -0.23 | -0.14 |
| m_7 | Summer greendown | 0.46 | -0.18 | -0.36 | 0.21 | -0.21 | 1.00 | 0.61 | -0.25 |
| MAX _{VEG} | Maximum vegetation cover | 0.16 | -0.09 | -0.14 | -0.22 | -0.23 | 0.61 | 1.00 | -0.11 |
| m_1 | Minimum vegetation cover | -0.18 | 0.04 | 0.12 | 0.01 | -0.14 | -0.25 | -0.11 | 1.00 |

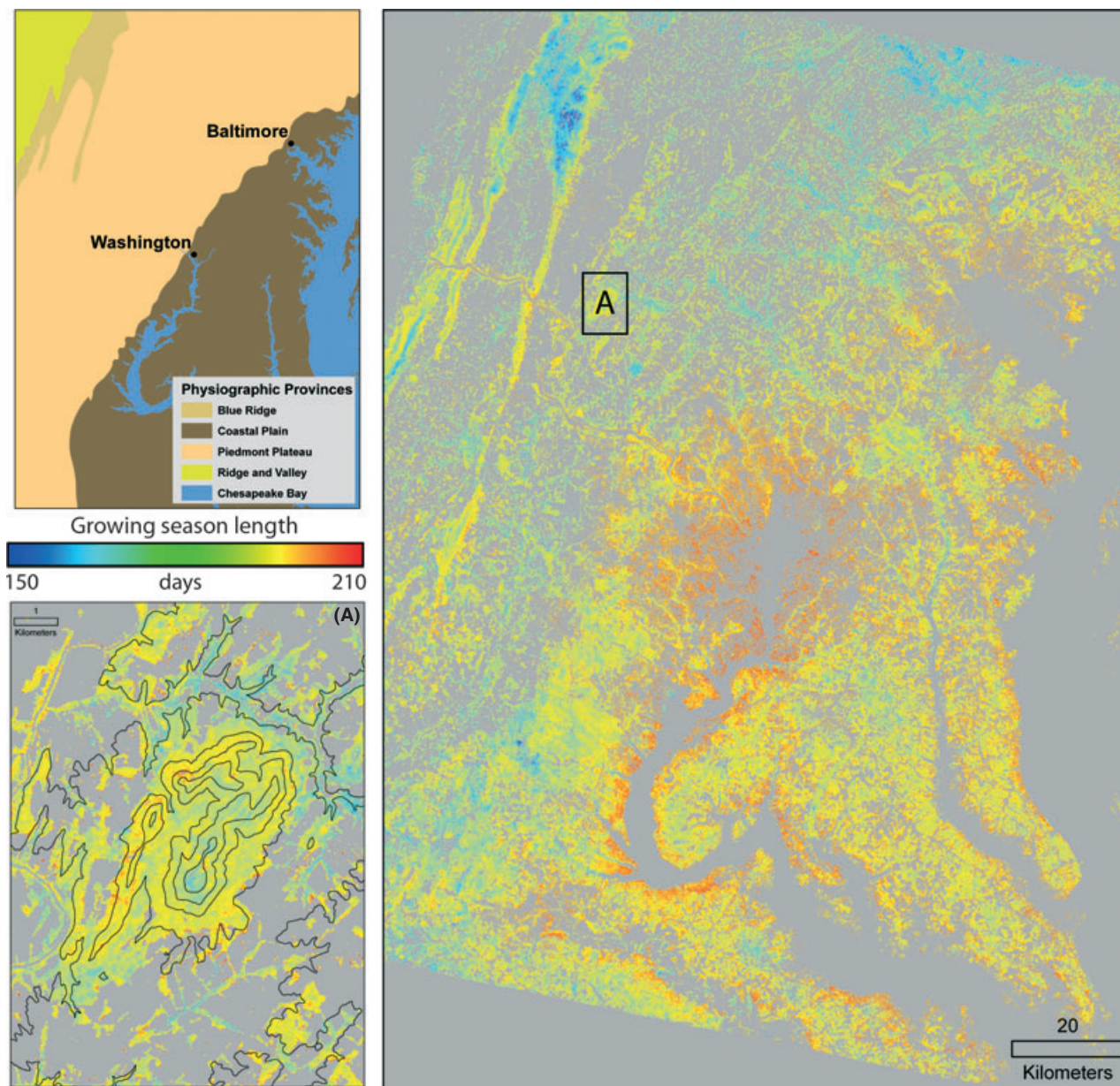


Fig. 8 Growing season length for forests in the study region across four physiographic provinces (upper left). Inset (a) shows detail for Sugar Loaf Mountain (255 m) with 50 m contour intervals shown from 50 m to 250 m. Across the study region, longer growing seasons are spatially related to lower elevations, coastal regions, and proximity to urban centers.

related to important traits such as decreasing net photosynthesis, leaf nitrogen (N), and specific leaf area (Reich *et al.*, 1997). Other efforts have attempted to link leaf chemistry to physiological traits and stand-level carbon assimilation (Field, 1983; Reich *et al.*, 1991; Wilson *et al.*, 2000; Ollinger *et al.*, 2008). At the scale of individual leaves, summer greendown is thus described as a gradual process related to aging and damage or stress. It often commences within weeks of initial leaf expansion. As leaves age they thicken and photosynthetic capacity decreases as mesophyll conductance and leaf nitrogen

allocated to photosynthetic machinery both decrease (Poorter & Evans, 1998; Rey & Jarvis, 1998; Wilson *et al.*, 2000). Through the growing season, light use efficiency decreases, but water use efficiency increases, suggesting that this process may be an adaptive response to reduced soil moisture in the late summer (Field & Mooney, 1983). Although there are few studies that investigate trends in leaf and canopy reflectance throughout the growing season, reduced contrast between the red and near-infrared wavelengths appears to be a consistent observation (Gausman *et al.*,

Table 3 Model results relating the spring onset, autumn offset, and growing season length to elevation, distance to tidal water, degree of urban (%ISA in vicinity), and latitude. Cp, Pp, and Br refer to the Coastal Plain, Piedmont Plateau, and Blue Ridge, respectively. For % Model SS, bold indicates significance ($P < 0.05$)

| | % Model SS | | | Estimates | | | P-value | | |
|---|--------------|--------------|--------------|-----------------|-----------------|-----------------|---------|--------|--------|
| | Cp | Pp | Br | Cp | Pp | Br | Cp | Pp | Br |
| Spring onset | | | | | | | | | |
| Intercept | 6.3% | 38.9% | 0.9% | 294 ± 35 | 954 ± 41 | 1540 ± 316 | <0.001 | <0.001 | <0.001 |
| Elevation (day 100 m ⁻¹) | 13.2% | 4.9% | 95.4% | -2.5 ± 20.39 | 0.64 ± 7.72 | 3.27 ± 6.42 | <0.001 | <0.001 | <0.001 |
| Tidal distance (day km ⁻¹) | 59.9% | 5.8% | 0.5% | 0.2 ± 7.676 | 0.065 ± 7.19 | 0.138 ± 37.019 | <0.001 | <0.001 | <0.001 |
| ISA (d%ISA-1) | 8.7% | 17.1% | 0.3% | -0.059 ± 0.006 | -0.093 ± 0.006 | -0.145 ± 0.051 | <0.001 | <0.001 | 0.0040 |
| Latitude (day km ⁻¹) | 2.4% | 31.9% | 0.8% | -0.043 ± 8.148 | -0.194 ± 9.233 | -0.336 ± 72.993 | <0.001 | <0.001 | <0.001 |
| Aspect (d deg) | 9.6% | 1.4% | 2.2% | 0.006 ± 0.001 | 0.003 ± 0.001 | 0.009 ± 0.001 | <0.001 | <0.001 | <0.001 |
| Model r ² | 0.12 | 0.22 | 0.74 | | | | | | |
| Autumn offset | | | | | | | | | |
| Intercept | 0.1% | 4.2% | 0.6% | 36 ± 49 | -371±55 | 472 ± 488 | 0.4600 | <0.001 | 0.3330 |
| Elevation (day 100m ⁻¹) | 11.6% | 37.6% | 74.7% | 3.21 ± 28.73 | 2.09 ± 10.39 | -1.09 ± 9.93 | <0.001 | <0.001 | <0.001 |
| Tidal distance (day km ⁻¹) | 58.7% | 4.3% | 17.8% | -0.272 ± 10.817 | -0.066 ± 9.676 | -0.306 ± 57.22 | <0.001 | <0.001 | <0.001 |
| ISA (d%ISA-1) | 24.4% | 37.6% | 5.3% | 0.135 ± 0.008 | 0.163 ± 0.008 | 0.23 ± 0.078 | <0.001 | <0.001 | 0.003 |
| Latitude (day km ⁻¹) | 2.7% | 14.5% | 0.0% | 0.062 ± 11.482 | 0.155 ± 12.425 | -0.02 ± 112.825 | <0.001 | <0.001 | 0.8560 |
| Aspect (d deg) | 2.4% | 1.8% | 1.6% | -0.004 ± 0.001 | 0.004 ± 0.001 | 0.003 ± 0.002 | <0.001 | <0.001 | 0.1060 |
| Model r ² | 0.07 | 0.11 | 0.18 | | | | | | |
| Growing season length | | | | | | | | | |
| Intercept | 0.9% | 21.0% | 0.2% | -258 ± 68 | -1325 ± 80 | -1067 ± 659 | <0.001 | <0.001 | 0.1060 |
| Elevation (day 100 m ⁻¹) | 12.7% | 7.1% | 94.7% | 5.71 ± 40.07 | 1.45 ± 14.97 | -4.35 ± 13.4 | <0.001 | <0.001 | <0.001 |
| Tidal distance (day km ⁻¹) | 61.3% | 6.6% | 3.0% | -0.472 ± 15.086 | -0.131 ± 13.942 | -0.444 ± 77.26 | <0.001 | <0.001 | <0.001 |
| ISA (d%ISA-1) | 17.4% | 36.3% | 1.1% | 0.194 ± 0.012 | 0.256 ± 0.012 | 0.375 ± 0.106 | <0.001 | <0.001 | <0.001 |
| Latitude (day km ⁻¹) | 2.7% | 28.9% | 0.4% | 0.105 ± 16.014 | 0.35 ± 17.903 | 0.315 ± 152.339 | <0.001 | <0.001 | 0.0390 |
| Aspect (d deg) | 5.0% | 0.0% | 0.5% | -0.01±0.001 | 0.001±0.001 | -0.006±0.002 | <0.001 | <0.001 | 0.4340 |
| Model r ² | 0.10 | 0.19 | 0.57 | | | | | | |

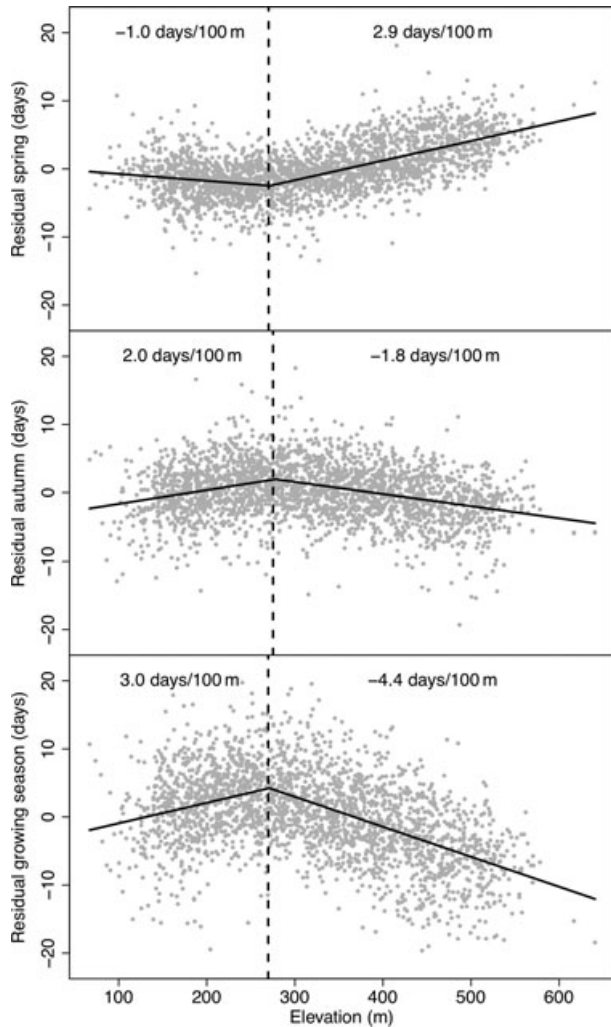


Fig. 9 Relationships between the spring onset, autumn offset, and growing season length and elevation in the Blue Ridge Mountains. In all three relationships, we calculated a model using all the variables in Table 3 with the exception of elevation and then plotted the residuals. Segmented regression was used to identify breakpoints in each relationship and the slope (indicated on each plot) of each linear segment. All values for slope, between segments and between variables, are significantly different in that their 95% standard errors do not overlap.

1971; Carter *et al.*, 1989), as does reduced contrast between the visible green and red wavelengths (Fig. 7a). Seasonal changes in leaf-level reflectance in the visible wavelengths are primarily related to synthesis and decay of foliar pigments (e.g. chlorophylls and carotenoids). Once leaf expansion is complete, reflectance in the visible red appears to change little until autumn senescence, at which time it increases as chlorophyll degrades rapidly (Fig. 2). In the near-infrared, however, reflectance declines throughout the summer (Jenkins *et al.*, 2007), thus influencing remote sensing measures of photosynthetic capacity.

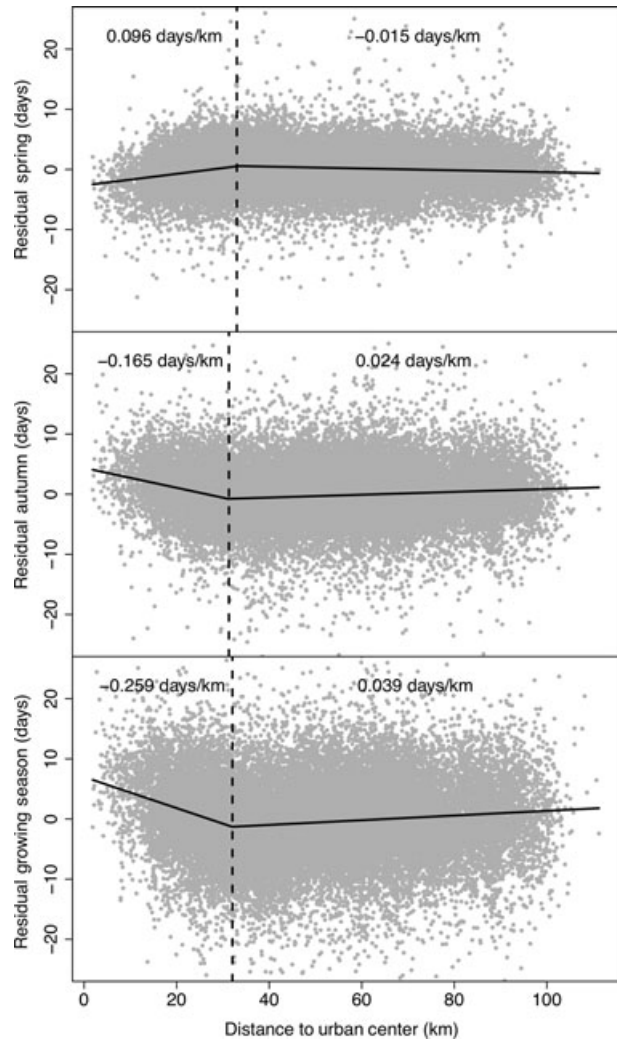


Fig. 10 Similar to Fig. 9, but showing relationships between the spring onset, autumn offset, and growing season length and distance to the urban centers of Baltimore and Washington, DC in the Piedmont and Coastal Plain.

Because greendown is a consistent feature of remote sensing timeseries, the 6-parameter logistic model, which assumes constant greenness throughout the summer, does not properly model forest canopy phenology. Our results show that transition to a 7-parameter model that explicitly models summer greendown is warranted and leads to improvements, both in terms of model parameter uncertainty and reduction in bias. Because greendown varies across the landscape, its influence on measurements of spring and autumn timing also varies over space. Thus by correctly modeling summer greendown, our approach enables a more accurate view of phenological patterns. A second technological advancement we introduce is refinement in the application of inverse modeling to stacks of high resolution remote sensing data organized by DOY. While this method

does not allow for analysis of interannual variability, it does provide a fine-grain analysis of the average date of spring onset and autumn offset of greenness that is relatively insensitive to data noise introduced by atmospheric and other ephemeral impacts common to remote sensing timeseries. In future work, annual deviations from the average phenology observed at any one point in time could be explored, which should theoretically be related to annual climate anomalies. If extended to fine-resolution remote sensing data (e.g. Quickbird, Ikonos, or webcam imagery) or different biophysical measurements from Landsat-class data, our methods could provide new inroads in phenological research that has long been concerned primarily with continental-scale patterns of leaf area and thus broad-scale climatic drivers (White *et al.*, 2009).

In mid-Atlantic forests, the effect of landscape factors on the timing of spring onset and autumn offset and growing season length is more complex than previously thought. Landscape variables were more successful in explaining variation in the spring onset (r^2 between 0.12 and 0.74) than in the autumn offset (r^2 between 0.07 and 0.18; Table 3) reflecting either increased uncertainty in values for the autumn offset relative to the spring onset (Table 1), or a generally reduced dependence on the landscape variables measured here. Previous work has indeed identified a stronger relationship between climate and the timing of spring relative to autumn. For example, both gross and net ecosystem productivity were more highly correlated with spring than autumn temperature anomalies in an analysis of eddy covariance flux tower data (FLUXNET), and remote sensing observations of canopy phenology were more highly correlated with dates of net carbon assimilation in spring than in autumn (Richardson *et al.*, 2010). Such observations have been attributed to decreasing light levels in autumn, reducing the productivity associated with extended growing seasons (Suni *et al.*, 2003). Observations that corroborate these past results were identified in the Blue Ridge Mountains, where higher elevations were associated with a later spring to a greater extent than an earlier autumn (Fig. 9). However, in other areas of our study region we found the opposite trend, that autumn offset was a stronger influence on growing season length than was spring onset. For example, for the region surrounding the cities of Baltimore and Washington, DC, increasing distance from these cities was associated with a stronger gradient in autumn offset than spring onset (Fig. 10). We found this gradient extended 32 km from the geographic center of these cities, approximately two times the distance observed in previous work utilizing coarse resolution data (Zhang *et al.*, 2004). Future work will have to explore

why urban heat islands might affect the timing of autumn more than the timing of spring, but candidate hypotheses might include changes in plant community composition (Shustack *et al.*, 2009) and reduced soil moisture limitations in cities where irrigation might be more common.

A second unexpected result was the finding of a breakpoint in the relationship between the timing of spring onset or autumn offset, and elevation located at 275 m (Fig. 9). Across the entire Blue Ridge elevation gradient (i.e. without considering the breakpoint) the observed relationship between the spring onset of greenness and elevation was 3.27 days 100 m^{-1} (Table 3), which generally matches what has been found previously. For example, studies of forests along the east coast, USA have found 2.7 days 100 m^{-1} (New Hampshire; Richardson *et al.*, 2006), 3.3 days 100 m^{-1} (mid-Atlantic; Hopkins, 1918), and 3.4 days 100 m^{-1} (North Carolina; Hwang *et al.*, 2011). The finer-grain of our data enables an investigation of how the relationship with elevation varies along different segments of the slope. We found that for the first 200 m of elevation increase, the spring onset actually became earlier by ~ 1 day 100 m^{-1} . This effect was even stronger in the autumn, leading to a strong breakpoint in the trend in growing season length with elevation (Fig. 9). The remaining elevation range above 275 m exhibited a trend of 2.7 days 100 m^{-1} , closely matching field observations in New Hampshire, USA (Richardson *et al.*, 2006). Recent work has highlighted complexities in the relationship between the onset of spring and elevation. For example, in southeast New England, a strong dependence on elevation was found in small areas where cold air drainage delayed the onset of greenness by approximately 25 days 100 m^{-1} (Fisher *et al.*, 2006). At larger scales, work has shown that the thermal time requirement for the spring onset of greenness increases with decreasing winter chilling days (Zhang *et al.*, 2007). In addition to these potential causes for the observed breakpoint (i.e. cold air drainage and sufficiently warm winters at lower elevations to require a longer thermal time requirement for spring onset of greenness), it might also be useful to consider the position of the atmospheric boundary layer, which might limit the effect of elevation on climate below ~ 275 m. The 275-m breakpoint does not coincide with any known transition in plant composition, such as to evergreen forest, but due to a general lack of information on plant community composition at this scale, such an effect cannot be completely ruled out.

We also found considerable residual variance that was unexplained by the landscape variables used here. Spatial autocorrelation in the residuals for both spring onset and autumn offset did not help us to identify

additional landscape variables to include in the model, suggesting that residual variance is simply data noise. Alternatively, residual variance might be explained by variables that are difficult to map at a fine spatial grain, such as species composition and edaphic factors (Liang *et al.*, 2011). Tree species are known to exhibit relatively consistent offsets in year-to-year phenological timing despite large inter-annual variability in observed transition dates and the underlying meteorological drivers (Richardson & O'Keefe, 2009). Analyses that utilize phenology data at a high spatial grain could potentially leverage from these differences to aid in species distribution mapping. Such interactions are generally obscured at coarse resolutions (e.g. 250 m to 1 km grain) due to mixed pixel effects with other land cover types.

Conclusions

The effects of climate change on forest ecosystem productivity will likely involve both changes in growing season length as well as site suitability, thus requiring analyses that consider changes in ecosystem processes during spring and autumn as well as trends throughout the summer. Summer greendown is biologically relevant in that it is clearly associated with ecological processes that vary across landscapes. Further, in webcam observations the rate of summer greendown appears to vary between years (Richardson *et al.*, 2009a; Fig 7a), suggesting annual climate factors are important in controlling the rate of summer green down. Therefore, if summer greendown intensifies (or is reduced) as a consequence of changes in drought or temperature stress, and this change is not accounted for in phenology models, estimates of autumn timing will become increasingly biased. Comprehensive analyses of forest productivity must include summer greenness trajectories as well as spring and autumn timing. We found, for example, that the maximum vegetation cover and the rate of summer greendown varied spatially, independent of spatial variations in the date of spring onset and autumn offset of greenness. This suggests complexity and tradeoffs in relationships between forest canopy greenness and growing season length that are entirely obscured if observations focus on just one time of year or assume constant leaf area throughout the year.

Transferring an understanding of the effect of landscape gradients on phenological timing to an understanding of the effect of temporal changes in climate is inherently problematic. The analysis of gradients provides insight into how ecosystem processes vary with climate-related variables, but these gradients also include hidden gradients in site characteristics that are difficult to measure using remote sensing

data (e.g. plant composition, edaphic factors, etc. Burke *et al.*, 1997). Nevertheless, studies that utilize space-for-time substitution along relatively short gradients (enabled by medium-grain remote sensing data) provide insight into how gradual changes in climate might influence phenological timing. We found that growing season length does not decrease linearly with increasing elevation, suggesting phenological responses to projected warming may not be as simple as an increase in growing season length and might depend strongly on microclimate (Fisher *et al.*, 2006; Hwang *et al.*, 2011), winter chilling requirements (Zhang *et al.*, 2007), and photoperiod (Korner & Basler, 2010). Secondly, we found that urban heat islands, centered on the two large cities in our study region, influenced the timing of autumn more strongly than the timing of spring, suggesting a diverse response to the warming (and associated changes in site characteristics) associated with the creation of urban forest fragments. As phenological data acquired at finer spatial grains become more common, future studies might examine more fully the ecosystem-level implications for these observed trends, and the degree to which they are upheld in forested systems worldwide.

Acknowledgements

We thank Dr Jeremy Fisher for insightful conversations during the early stages of this work, the Northeastern States Research Cooperative for supporting the PhenoCam network, and the National Park Service for contributing imagery from the National Capitol camera to the PhenoCam image archive. This is University of Maryland Center for Environmental Science scientific contribution #4540.

References

- Adams JB, Smith MO, Johnson PE (1986) Spectral mixture modeling: a new analysis of rock and soil types at the Viking Lander I Site. *Journal of Geophysical Research*, **91**, 8098–8112.
- Ahas R, Aasa A, Menzel A, Fedotova V, Scheffinger H (2002) Changes in European spring phenology. *International Journal of Climatology*, **22**, 1727–1738.
- Ahrens HE, Brügger R, Stöckli R *et al.* (2008) Quantitative phenological observations of a mixed beech forest in northern Switzerland with digital photography. *Journal of Geophysical Research-Biogeosciences*, **113**, G04004, doi: 10.1029/2007JG000650.
- Asner GP, Hicke JA, Lobell DB (2003) Per-pixel analysis of forest structure: vegetation indices, spectral mixture analysis and canopy reflectance modeling. In: *Remote Sensing of Forest Environments: Concepts and Case Studies* (eds Wulder MA, Franklin SE), pp. 209–254. Kluwer Academic publishers, Boston, MA.
- Asner GP, Elmore AJ, Olander LP, Martin R, Harris AT (2004) Grazing systems, ecosystem interactions, and global change. *Annual Review of Environment and Resources*, **29**, 11.11–11.39.
- Baldocchi DD, Wilson KB (2001) Modeling CO₂ and water vapor exchange of a temperate broadleaved forest across hourly to decadal time scales. *Ecological Modelling*, **142**, 155–184.
- Bradley BA, Jacob RW, Hermance JF, Mustard JF (2007) A curve fitting procedure to derive inter-annual phenologies from time series of noisy satellite NDVI data. *Remote Sensing of Environment*, **106**, 137–145.

- Brown SL, Schroeder P, Kern JS (1999) Spatial distribution of biomass in forests of the eastern USA. *Forest Ecology and Management*, **123**, 81–90.
- Brügger R, Studer S, Stöckli R (2007) Die Vegetationsentwicklungserfasst am Individuum und über den Raum (Changes in plant development monitored on the individual plant and over geographical area). *Schweiz Z Forstwes*, **158**, 221–228.
- Burke IC, Lauenroth WK, Parton WJ (1997) Regional and temporal variation in net primary production and nitrogen mineralization in grasslands. *Ecology*, **78**, 1330–1340.
- Carter GA, Paliwal K, Pathre U, Green TH, Mitchell RJ, Gjerstad DH (1989) Effect of competition and leaf age on visible and infrared reflectance in pine foliage. *Plant, Cell and Environment*, **12**, 309–315.
- Chapin FS, Randerson JT, McGuire AD, Foley JA, Field CB (2008) Changing feedbacks in the climate-biosphere system. *Frontiers in Ecology and Environment*, **6**, 313–320.
- Chastain RA, Townsend PA (2008) Role of evergreen understory shrub layer in the forests of the central Appalachian Highlands. *Journal of the Torrey Botanical Society*, **135**, 208–223.
- Chmielewski FM, Rotzer T (2002) Annual and spatial variability of the beginning of the growing season in Europe in relation to air temperature changes. *Climate Research*, **19**, 257–264.
- Christidis N, Stott PA, Brown S, Karoly DJ, Caesar J (2007) Human contribution to the lengthening of the growing season during 1950–99. *Journal of Climate*, **20**, 5441–5454.
- Efron B (1979) 1977 rietz lecture – bootstrap methods – another look at the jackknife. *Annals of Statistics*, **7**, 1–26.
- Efron B, Tibshirani R (1991) Statistical-data analysis in the computer-age. *Science*, **253**, 390–395.
- Elmore AJ, Craine JM (2011) Spectroscopic analysis of canopy nitrogen and nitrogen isotopes in managed pastures and hay land. *Transactions on Geoscience and Remote Sensing*, **49**, 2491–2498.
- Elmore AJ, Guinn SM (2010) Synergistic use of Landsat Multispectral Scanner with GIRAS land-cover data to retrieve impervious surface area for the Potomac River Basin in 1975. *Remote Sensing of Environment*, **114**, 2384–2391.
- Elmore AJ, Mustard JF, Manning SJ, Lobell DB (2000) Quantifying vegetation change in semiarid environments: precision and accuracy of spectral mixture analysis and the Normalized Difference Vegetation Index. *Remote Sensing of Environment*, **73**, 87–102.
- Farquharson CG, Oldenburg DW (1998) Non-linear inversion using general measures of data misfit and model structure. *Geophysical Journal International*, **134**, 213–227.
- Field C (1983) Allocating leaf nitrogen for the maximization of carbon gain: leaf age as a control on the allocation program. *Oecologia*, **56**, 341–347.
- Field C, Mooney HA (1983) Leaf age and seasonal effects on light, water, and nitrogen use efficiency in a California shrub. *Oecologia*, **56**, 348–355.
- Field CB, Lobell DB, Peters HA, Chiariello NR (2007) Feedbacks of terrestrial ecosystems to climate change. *Annual Review of Environment and Resources*, **32**, 1–29.
- Fisher JJ, Mustard JF (2007) Cross-scalar satellite phenology from ground, Landsat, and MODIS data. *Remote Sensing of Environment*, **109**, 261–273.
- Fisher JJ, Mustard JF, Vadeboncoeur MA (2006) Green leaf phenology at Landsat resolution: scaling from the field to the satellite. *Remote Sensing of Environment*, **100**, 265–279.
- Fisher JJ, Richardson AD, Mustard JF (2007) Phenology model from surface meteorology does not capture satellite-based greenup estimations. *Global Change Biology*, **13**, 707–721.
- Fitzjarrald DR, Ocevedo OC, Moore KE (2001) Climatic consequences of leaf presence in the eastern United States. *Journal of Climate*, **14**, 598–614.
- Friedl MA, Sulla-Menashe D, Tan B, Schneider A, Ramankutty N, Sibley A, Huang XM (2010) MODIS Collection 5 global land cover: algorithm refinements and characterization of new datasets. *Remote Sensing of Environment*, **114**, 168–182.
- Ganguly S, Friedl MA, Tan B, Zhang X, Verma M (2010) Land surface phenology from MODIS: characterization of the Collection 5 Global Land Cover Dynamics Product. *Remote Sensing of Environment*, **114**, 1805–1816.
- Gausman HW, Allen WA, Escobar DE, Rodriguez RR, Cardenas R (1971) Age effects of cotton leaves on light reflectance, transmittance, and absorbance and on water content and thickness. *Agronomy Journal*, **63**, 465–469.
- Gazal R, White MA, Gillies R, Rodemaker E, Sparrow E, Gordon L (2008) GLOBE students, teachers, and scientists demonstrate variable differences between urban and rural leaf phenology. *Global Change Biology*, **14**, 1568–1580.
- Gu D, Gillespie AR (1998) Topographic normalization of Landsat TM images of forest based on subpixel sun-canopy-sensor geometry. *Remote Sensing of Environment*, **64**, 166–175.
- Gu L, Post WM, Baldocchi D, Black TA, Verma SB, Vesala T, Wofsy SC (2003) Phenology of vegetation photosynthesis. In: *Phenology: An Integrative Environmental Science* (ed. Schwartz MD), pp. 467–486. Kluwer, Dordrecht.
- Hopkins AD (1918) Periodical events and natural law as guides to agricultural research and practice. *Monthly Weather Review*, **9** (Suppl.), 1–42.
- Hwang T, Song CH, Vose JM, Band LE (2011) Topography-mediated controls on local vegetation phenology estimated from MODIS vegetation index. *Landscape Ecology*, **26**, 541–556.
- Imhoff ML, Zhang P, Wolfe RE, Bounoua L (2010) Remote sensing of the urban heat island effect across biomes in the continental USA. *Remote Sensing of Environment*, **114**, 504–513.
- Irish RR, Barker JL, Goward SN, Arvidson TJ (2006) Characterization of the Landsat-7 Automated Cloud-Cover Assessment (ACCA) Algorithm. *Photogrammetric Engineering and Remote Sensing*, **70**, 1179–1188.
- Jenkins JC, Birdsey RA, Pan Y (2001) Biomass and NPP estimation for the mid-Atlantic region (USA) using plot-level forest inventory data. *Ecological Applications*, **11**, 1174–1193.
- Jenkins JP, Richardson AD, Braswell BH, Ollinger SV, Hollinger DY, Smith ML (2007) Refining light-use efficiency calculations for a deciduous forest canopy using simultaneous tower-based carbon flux and radiometric measurements. *Agricultural and Forest Meteorology*, **143**, 64–79.
- Korner C, Basler D (2010) Warming, photoperiods, and tree phenology response. *Science*, **329**, 278–278.
- Lechowicz MJ (1984) Why do temperate deciduous trees leaf out at different times? Adaptation and ecology of forest communities. *American Naturalist*, **124**, 831–842.
- Liang L, Schwartz M (2009) Landscape phenology: an integrative approach to seasonal vegetation dynamics. *Landscape Ecology*, **24**, 465–472.
- Liang LA, Schwartz MD, Fei SL (2011) Validating satellite phenology through intensive ground observation and landscape scaling in a mixed seasonal forest. *Remote Sensing of Environment*, **115**, 143–157.
- Lichstein JW, Simons TR, Shriver SA, Franzreb KE (2002) Spatial autocorrelation and autoregressive models in ecology. *Ecological Monographs*, **72**, 445–463.
- Lobell DB, Asner GP, Law BE, Treuhart RN (2001) Subpixel canopy cover estimation of coniferous forests in Oregon using SWIR imaging spectrometry. *Journal of Geophysical Research-Atmospheres*, **106**, 5151–5160.
- Lookingbill TR, Kaushal SS, Elmore AJ *et al.* (2009) Altered ecological flows blur boundaries in urbanizing watersheds. *Ecology and Society*, **14**, 10.
- Masek JG, Vermote EF, Saleous NE *et al.* (2006) A Landsat surface reflectance dataset for North America, 1990–2000. *IEEE Geoscience and Remote Sensing Letters*, **3**, 68–72.
- Menke W (1989) *Geophysical Data Analysis: Discrete Inverse Theory*. Academic Press, Inc., San Diego, CA.
- Menzel A, Fabian P (1999) Growing season extended in Europe. *Nature*, **397**, 659–660.
- Minor ES, Tessel SM, Engelhardt KAM, Lookingbill TR (2009) The role of landscape connectivity in assembling exotic plant communities: a network analysis. *Ecology*, **90**, 1802–1809.
- Morisette JT, Richardson AD, Knapp AK *et al.* (2009) Tracking the rhythm of the seasons in the face of global change: phenological research in the 21st century. *Frontiers in Ecology and the Environment*, **7**, 253–260.
- Mustard JF (1993) Relationships of soil, grass, and bedrock over the Kaweah Serpentine Melange through spectral mixture analysis of Aviris data. *Remote Sensing of Environment*, **44**, 293–308.
- Myneni RB, Keeling CD, Tucker CJ, Asrar G, Nemani RR (1997) Increased plant growth in the northern high latitudes from 1981 to 1991. *Nature*, **386**, 698–702.
- Naik SK, Murthy CA (2003) Hue-preserving color image enhancement without gamut problem. *IEEE Transactions on Image Processing*, **12**, 1591–1598.
- Najjar RG, Pyke CR, Adams MB *et al.* (2010) Potential climate-change impacts on the Chesapeake Bay. *Estuarine Coastal and Shelf Science*, **86**, 1–20.
- Noormets A (2009) *Phenology of Ecosystem Processes*. Springer, New York.
- Ollinger SV, Richardson AD, Martin ME *et al.* (2008) Canopy nitrogen, carbon assimilation, and albedo in temperate and boreal forests: functional relations and potential climate feedbacks. *Proceedings of the National Academy of Sciences USA*, **105**, 19336–19341.
- Parker RL, McNutt MK (1980) Statistics for the one-norm misfit measure. *Journal of Geophysical Research*, **85**, 4429–4430.
- Parmesan C, Yohe G (2003) A globally coherent fingerprint of climate change impacts across natural systems. *Nature*, **421**, 37–42.

- Piao SL, Friedlingstein P, Ciais P, Viovy N, Demarty J (2007) Growing season extension and its impact on terrestrial carbon cycle in the Northern Hemisphere over the past 2 decades. *Global Biogeochemical Cycles*, **21**, GB3018, doi: 10.1029/2006GB002888.
- Piao SL, Ciais P, Friedlingstein P *et al.* (2008) Net carbon dioxide losses of northern ecosystems in response to autumn warming. *Nature*, **451**, 49–52.
- Poorter H, Evans JR (1998) Photosynthetic nitrogen-use efficiency of species that differ inherently in specific leaf area. *Oecologia*, **116**, 26–37.
- Reich PB, Walters MB, Ellsworth DS (1991) Leaf age and season influence the relationships between leaf nitrogen, leaf mass per area and photosynthesis in maple and oak trees. *Plant, Cell and Environment*, **14**, 251–259.
- Reich PB, Walters MB, Ellsworth DS (1997) From tropics to tundra: Global convergence in plant functioning. *Proceedings of the National Academy of Sciences of the United States of America*, **94**, 13730–13734.
- Rey A, Jarvis PG (1998) Long-term photosynthetic acclimation to increased atmospheric CO₂ concentration in young birch (*Betula pendula*) trees. *Tree Physiology*, **18**, 441–450.
- Richardson AD, O'Keefe J (2009) Phenological differences between understory and overstory: A case study using the long-term Harvard forest records. In: *Phenology of Ecosystem Processes* (ed. Noormets A), pp. 87–117. Springer, New York.
- Richardson AD, Bailey AS, Denny EG, Martin CW, O'Keefe J (2006) Phenology of a northern hardwood forest canopy. *Global Change Biology*, **12**, 1174–1188.
- Richardson AD, Jenkins JP, Braswell BH, Hollinger DY, Ollinger SV, Smith ML (2007) Use of digital webcam images to track spring green-up in a deciduous broadleaf forest. *Oecologia*, **152**, 323–334.
- Richardson AD, Braswell BH, Hollinger DY, Jenkins JP, Ollinger SV (2009a) Near-surface remote sensing of spatial and temporal variation in canopy phenology. *Ecological Applications*, **19**, 1417–1428.
- Richardson AD, Hollinger DY, Dail DB, Lee JT, Munger JW, O'Keefe J (2009b) Influence of spring phenology on seasonal and annual carbon balance in two contrasting New England forests. *Tree Physiology*, **29**, 321–331.
- Richardson AD, Black TA, Ciais P *et al.* (2010) Influence of spring and autumn phenological transitions on forest ecosystem productivity. *Philosophical Transactions of the Royal Society of London*, **365**, 3227–3246.
- Robeson SM (2002) Increasing growing-season length in Illinois during the 20th century. *Climatic Change*, **52**, 219–238.
- Scales JA, Gersztenkorn A, Treitel S (1988) Fast lp solution of large, sparse, linear systems: application to seismic travel time tomography. *Journal of Computational Physics*, **75**, 314–333.
- Schwartz MD, Ahas R, Aasa A (2006) Onset of spring starting earlier across the Northern Hemisphere. *Global Change Biology*, **12**, 343–351.
- Shustack DP, Rodewald AD, Waite TA (2009) Springtime in the city: exotic shrubs promote earlier greenup in urban forests. *Biological Invasions*, **11**, 1357–1371.
- Small C (2004) The landsat ETM plus spectral mixing space. *Remote Sensing of Environment*, **93**, 1–17.
- Smith MO, Ustin SL, Adams JB, Gillespie AR (1990) Vegetation in deserts: I. A regional measure of abundance from multispectral images. *Remote Sensing of Environment*, **31**, 1–26.
- Song C, Woodcock CE, Seto KC, Lenney MP, Macomber SA (2001) Classification and change detection using Landsat TM data: When and how to correct atmospheric effects? *Remote Sensing of Environment*, **75**, 230–244.
- Suni T, Berninger F, Markkanen T, Keronen P, Rannik U, Vesala T (2003) Interannual variability and timing of growing-season CO₂ exchange in a boreal forest. *Journal of Geophysical Research - Atmospheres*, **108**, 4265.
- Tuanmu M, Vina A, Bearer S, Xu W, Ouyang Z, Zhang H, Liu J (2010) Mapping understory vegetation using phenological characteristics derived from remotely sensed data. *Remote Sensing of Environment*, **114**, 1833–1844.
- Vitasse Y, Porte AJ, Kremer A, Michalet R, Delzon S (2009) Responses of canopy duration to temperature changes in four temperate tree species: relative contributions of spring and autumn leaf phenology. *Oecologia*, **161**, 187–198.
- Wang ZJ, Ziou D, Armenakis C, Li D, Li QQ (2005) A comparative analysis of image fusion methods. *IEEE Transactions on Geoscience and Remote Sensing*, **43**, 1391–1402.
- White MA, Nemani AR (2003) Canopy duration has little influence on annual carbon storage in the deciduous broad leaf forest. *Global Change Biology*, **9**, 967–972.
- White MA, de Beurs KM, Didan K *et al.* (2009) Intercomparison, interpretation, and assessment of spring phenology in North America estimated from remote sensing for 1982–2006. *Global Change Biology*, **15**, 2335–2359.
- Wilfong BN, Gorchov DL, Henry MC (2009) Detecting an invasive shrub in deciduous forest understories using remote sensing. *Weed Science*, **57**, 512–520.
- Wilson KB, Baldocchi DD, Hanson PJ (2000) Spatial and seasonal variability of photosynthetic parameters and their relationship to leaf nitrogen in a deciduous forest. *Tree Physiology*, **20**, 565–578.
- Woodcock CE, Allen R, Anderson M *et al.* (2008) Free access to Landsat imagery. *Science*, **320**, 1011.
- Zhang XY, Friedl MA, Schaaf CB *et al.* (2003) Monitoring vegetation phenology using MODIS. *Remote Sensing of Environment*, **84**, 471–475.
- Zhang X, Friedl MA, Schaaf CB, Strahler AH, Schneider A (2004) The footprint of urban climates on vegetation phenology. *Geophysical Research Letters*, **31**, 1–4.
- Zhang X, Tarpley D, Sullivan JT (2007) Diverse responses of vegetation phenology to a warming climate. *Geophysical Research Letters*, **34**, L19405.
- Zhao MS, Running SW (2010) Drought-induced reduction in global terrestrial net primary production from 2000 through 2009. *Science*, **329**, 940–943.